Photonics of time-varying media

Emanuele Galiffi [a,b,*] **Romain Tirole** [b,†] **Shixiong Yin** [a,†] **Huanan Li** [a,c] **Stefano Vezzoli**,[b] **Paloma A. Huidobro** [d] **Mário G. Silveirinha** [d] **Riccardo Sapienza** [b] **Andrea Alù** [a,e] **and J. B. Pendry** [b]

[a]City University of New York, Photonics Initiative, Advanced Science Research Center, New York, United States
[b]Imperial College London, Blackett Laboratory, Department of Physics, London, United Kingdom
[c]Nankai University, School of Physics, Tianjin, China
[d]Instituto de Telecomunicações, Instituto Superior Técnico-University of Lisbon, Lisboa, Portugal
[e]City University of New York, Physics Program, Graduate Center, New York, United States

Abstract. Time-varying media have recently emerged as a new paradigm for wave manipulation, due to the synergy between the discovery of highly nonlinear materials, such as epsilon-near-zero materials, and the quest for wave applications, such as magnet-free nonreciprocity, multimode light shaping, and ultrafast switching. In this review, we provide a comprehensive discussion of the recent progress achieved with photonic metamaterials whose properties stem from their modulation in time. We review the basic concepts underpinning temporal switching and its relation with spatial scattering and deploy the resulting insight to review photonic time-crystals and their emergent research avenues, such as topological and non-Hermitian physics. We then extend our discussion to account for spatiotemporal modulation and its applications to nonreciprocity, synthetic motion, giant anisotropy, amplification, and many other effects. Finally, we conclude with a review of the most attractive experimental avenues recently demonstrated and provide a few perspectives on emerging trends for future implementations of time-modulation in photonics.

Keywords: time-varying media; temporal modulation; metamaterials; switching; optics; photonics; light.

1 Introduction

In the wake of the extraordinary scientific advances of the last two centuries, the role of time underpins many of the unsolved puzzles of the physical world. In quantum theory, time is the only quantity not associated to an observable, being merely treated as a variable, while attempts to bring it to a common ground with all other physical quantities are still in the making.[1] Meanwhile, at cosmological scales, the measured acceleration of the expansion of the universe makes it hard to imagine a complete cosmological theory where temporal dynamics of, e.g., wave phenomena do not play a central role. Yet, most basic physics is carried out under the assumption that physical systems are passive, merely responding "after" any input stimuli.

Occasionally, the need to account for certain truly multiphysics or nonlinear phenomena brings up opportunities to develop our understanding of wave physics in temporally inhomogeneous systems; for instance, to realize bench-top analogs of relativistic phenomena, early attempts were made to tap into time-modulated classical wave systems.[2,3] However, the critical mass of research efforts needed to accomplish sizeable advances in this direction has, until recently, been lacking. On yet another front of exploration, time-crystals have been proposed in condensed matter theory for almost a decade as a stable state of matter capable of spontaneously breaking continuous time-translation symmetry while preserving long-range temporal order;[4] their very existence has been questioned and revised,[5] and several increasingly successful implementations have recently been accomplished.[6,7]

Meanwhile, over the past two decades, the rise of the field of metamaterials has proven how much fundamental wave physics lies untapped under the hood of well-established classical theories, such as electromagnetism, acoustics, and elasticity. Recently, the quest for novel forms of wave–matter interactions in these fields has led to a significant growth of interest in the exploration of time as a novel degree of freedom for

---

*Address all correspondence to Emanuele Galiffi, egaliffi@gc.cuny.edu

†These authors contributed equally to this work.

metamaterials.[8] In this pursuit, our need for even a basic understanding of wave phenomena in the time domain has been reflected in the wealth of surprising physical effects recently unveiled, largely theoretically and in part experimentally, which can be enabled by externally applying explicit temporal modulations on the parameters of a physical system.

In this review article, we present an overview of the state-of-the-art across the rapidly expanding field of time-varying photonic metamaterials in the hope that it may serve the photonics and metamaterials community as a catalyst for current and future explorations of this fascinating field. While not as detailed as a tutorial paper, the review aims at presenting the basic building blocks of time-varying electromagnetics, with the main goal of developing basic insight into the relevant phenomenology, while offering a broad view of key past and future research directions in the field.

The paper is structured as follows. Section 2 starts from the basics of electromagnetic time-switching, expanding toward more complex scenarios, such as as non-Hermitian and anisotropic switching, temporal slabs, and space–time interfaces. Section 3 is dedicated to photonic time-crystals (PTCs), namely electromagnetic systems undergoing infinite (periodic or disordered) modulations of their parameters in time-only, and we discuss some of its most promising directions toward, e.g., the engineering of topological phases, synthetic frequency dimensions, non-Hermitian physics, and localization, concluding with some perspective on the peculiarities of time-varying surfaces. Spatiotemporal crystals are discussed in Sec. 4, where we introduce the characteristic features of space–time band diagrams, homogenization procedures for traveling-wave modulated systems enabling effective-medium descriptions of synthetic motion, and highlight some recently emerged opportunities for nonreciprocity, synthetic Fresnel drag and wave amplification and compression, as well as space–time-modulated metasurfaces and some of their applications. Finally, Sec. 5 offers an overview of the most promising platforms for experimental implementations of time-modulation in photonics.

2 Wave Engineering with Temporal Interfaces

Light scattering by spatial interfaces [Fig. 1(a)] is the basis of many wave phenomena, from the simplest refraction effects to the complexity of wave engineering in complex media involving multilayers,[9] anisotropy,[10] nonlinearity,[11] extreme constitutive parameters,[12–14] or metamaterials and metasurfaces,[15] to name a few. How do electromagnetic waves behave when encountering interfaces in time rather than in space? Temporal interfaces can be created by abruptly switching the material properties of a medium in time, preserving its spatial continuity [Fig. 1(b)]. Wave propagation in switched media was first investigated by Morgenthaler in 1958.[16] In parallel, the study of light interactions with abruptly switched materials was developed in the plasma physics community, since the plasma permittivity can be switched in time by fast ionization processes.[17] In this section, we focus on the recent explorations of time-switching in photonic materials.

2.1 Temporal Boundary Conditions and Temporal Scattering

It is well known that wave propagation across spatial interfaces is governed by established boundary conditions; see, e.g.,
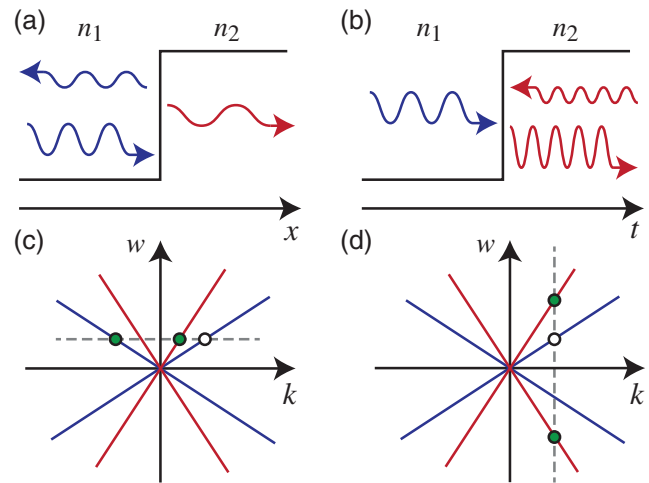

Fig. 1 Scattering at (a) a spatial discontinuity, generating transmitted and reflected waves propagating in different media with refractive indices n_1 and n_2, and (b) a temporal discontinuity, generating forward and backward waves propagating in the same medium. (c), (d) Illustration of the respective scattering processes on a dispersion diagram: the blue and red lines denote the dispersion cone for the two media. Note how the frequency ω is conserved in a spatial scattering process, and coupling occurs to forward and backward modes in the two different media, whereas in a time-scattering process the momentum k is conserved, and the two scattered waves are both embedded in the new medium.

Ref. 18. The essential constraint is that all relevant physical quantities, for instance, electric and magnetic fields (**E** and **H**), must be finite at all points in space and time. Spatial boundary conditions are therefore derived by integrating Maxwell's equations over an infinitesimal area and volume across the spatial interface, implying the continuity of tangential **E** and **H** at an interface that does not support surface current densities. Dually, the integration over a time interval across a temporal boundary obeys temporal boundary conditions. Let us start with the macroscopic Maxwell's curl equations:

$$\frac{\partial \mathbf{B}}{\partial t} = -\nabla \times \mathbf{E}, \tag{1}$$

$$\frac{\partial \mathbf{D}}{\partial t} = -\mathbf{J} + \nabla \times \mathbf{H}. \tag{2}$$

Here, we assume that the medium is unbounded and homogeneous before and after a switching instance at $t = t_0$. Integrating from $t_0^- = t_0 - \epsilon$ to $t_0^+ = t_0 + \epsilon$ with a $\epsilon \to 0^+$, we expect that the right-hand sides of Eqs. (1) and (2) are both zero, due to the finite values of fields and sources. Then, we obtain the temporal boundary conditions:

$$\mathbf{B}(t = t_0^+) = \mathbf{B}(t = t_0^-), \tag{3a}$$

$$\mathbf{D}(t = t_0^+) = \mathbf{D}(t = t_0^-). \tag{3b}$$

They ensure that the magnetic flux density **B** and the electric displacement **D** vary continuously in the time domain.

Alternatively, the continuity of **B** and **D** can also be interpreted by the conservation of magnetic flux Φ and electric charges Q, as shown by Morgenthaler[16] and Auld et al.,[19] respectively.

One of the most intriguing phenomena arising at a temporal discontinuity is the wave scattering dual to that occurring at spatial interfaces, producing forward and backward waves in time, rather than waves reflected and transmitted in space.[16,19–23] The scattering coefficients can be found by applying the above temporal boundary conditions. Consider a monochromatic plane wave traveling in an unbounded, homogeneous, isotropic, nondispersive but time-varying medium. Both permittivity ε and permeability μ are assumed to abruptly switch from their initial values ε_1 and μ_1 to ε_2 and μ_2 at $t = t_0$. We can denote the incident wave with $D_x = D_1 e^{j\omega_1 t - jkz}$ and $B_y = B_1 e^{j\omega_1 t - jkz}$, where ω_1 is the angular frequency and k is the wavenumber. The field amplitudes are related by $B_1 = Z_1 D_1$ with $Z_1 = \sqrt{\mu_1/\varepsilon_1}$. The fields after the switching event read

$$D_x(t > t_0) = [T e^{j\omega_2(t-t_0)} + R e^{-j\omega_2(t-t_0)}]D_1 e^{j(\omega_1 t_0 - k_2 z)}, \quad (4a)$$

$$B_y(t > t_0) = Z_2[T e^{j\omega_2(t-t_0)} - R e^{-j\omega_2(t-t_0)}]D_1 e^{j(\omega_1 t_0 - k_2 z)}. \quad (4b)$$

T and R are the transmission and reflection coefficients defined for the electric displacement field, and $Z_2 = \sqrt{\mu_2/\varepsilon_2}$ is the new wave impedance after switching. The temporal boundary conditions [Eq. (3)] need to be satisfied everywhere in space, which implies that $k_2 = k$, or equivalently

$$\omega_2 \sqrt{\varepsilon_2 \mu_2} = \omega_1 \sqrt{\varepsilon_1 \mu_1}. \quad (5)$$

This condition ensures momentum conservation across temporal interfaces, which is expected due to the preserved spatial homogeneity.[16,17,24,25] By equating the incident and scattered **D** and **B** fields at $t = t_0$, we solve for the temporal scattering coefficients:

$$T = \frac{Z_2 + Z_1}{2Z_2}, \quad (6a)$$

$$R = \frac{Z_2 - Z_1}{2Z_2}. \quad (6b)$$

The coefficients for the electric field can be easily found by substituting the constitutive relation between D and E, which are adopted more widely in the literature. It should be emphasized that the results presented in Eqs. (5) and (6) generally apply to an abrupt temporal interface under the assumptions of spatial homogeneity, isotropy, and instantaneous material response and may change if one or more of these assumptions are relaxed.[26] Illustrations of spatial and temporal scattering processes are shown in Figs. 1(a), 1(c) and 1(b), 1(d), respectively. As we consider more realistic and complicated electrodynamic models of materials, such as anisotropy, dispersion, and broken translational symmetry in space, the temporal scattering is expectedly modified.[27–33] To date, research on these topics is very active, as discussed in the following sections.

2.2 Temporal Slabs

Leveraging scattering phenomena at time interfaces, research efforts have been dedicated to the engineering of wave interference in time, for example, in the context of discrete time crystals[34–36] and time metamaterials.[37] Even when multiple temporal interfaces are involved, temporal interferences occur only between forward and backward waves induced by each boundary independently, due to the irreversibility of time, which introduces significant differences compared with spatial interfaces. A key contrast between spatial and temporal scattering from a mathematical standpoint is that space-scattering generally gives rise to boundary-value problems, whereas time-scattering leads to initial-value problems. Here, we discuss the recent progress in temporal slabs comprising one or two consecutive switching events. In Sec. 3, we discuss (quasi)periodically switched media.

The temporal interference introduced by a single temporal slab was first investigated by Mendonça et al.[38] Where they assume that the refractive index of a medium is switched from n_0 to n_1, and then switched back to n_0 after a time interval τ. The total transmission and reflection amplitudes were found to be

$$T_{\text{total}} = \left[\cos(\omega_1 \tau) + \frac{j}{2\alpha}(1 + \alpha^2)\sin(\omega_1 \tau)\right]e^{-j\omega_0 \tau}, \quad (7a)$$

$$R_{\text{total}} = -\frac{j}{2\alpha}(1 - \alpha^2)\sin(\omega_1 \tau)e^{j\omega_0 \tau}, \quad (7b)$$

where $\alpha = n_0/n_1$ and ω_0, ω_1 are the frequencies of waves outside and inside of the temporal slab, respectively. Similar results were also obtained using a quantum optics formulation, illustrating the probability of creating Fock states of photon pairs with opposite momentum from the vacuum state.[38] A temporal Fabry–Perot slab with dispersion was recently studied in Ref. 33. The most important phenomenon induced in these systems may arguably be the amplification of light. Because frequency and energy are not conserved at time boundaries, we can indeed expect a large amplification of the input energy at a suitably tailored temporal slab. It can be seen from Eq. (7) that such an amplification process attains the maximum level when the time interval $\omega_1 \tau$ is an odd multiple of $\pi/2$. On the contrary, time reflections can be minimized with $\sin(\omega \tau_1) = 0$. This finding can be connected to the dual phenomenon of impedance-matching layers in spatial scattering. Indeed, Pacheco-Peña and Engheta[39] recently introduced antireflection temporal coatings by proposing to rapidly change the permittivity of an unbounded medium twice, making an analogy to the quarter-wavelength impedance matching in the spatial domain. The schematic of such coatings is shown in Fig. 2(a). To minimize the backward reflection when the permittivity is to be switched from ε_1 to ε_2, they introduce a temporal coating with permittivity ε_{eq} and duration Δt in between. Impedance matching is enabled with

$$\varepsilon_{\text{eq}} = \sqrt{\varepsilon_1 \varepsilon_2}, \quad \Delta t = \frac{n T_{\text{eq}}}{4}; \quad n = 1, 3, 5, \ldots \quad (8)$$

where $T_{\text{eq}} = 1/f_{\text{eq}}$ is the equivalent period of the wave right after the permittivity is switched to ε_{eq} and the equivalent frequency $f_{\text{eq}} = \sqrt{\varepsilon_1/\varepsilon_{\text{eq}}}f_1$. A numerical simulation is shown in Fig. 2(b), indicating nearly vanishing reflection from the
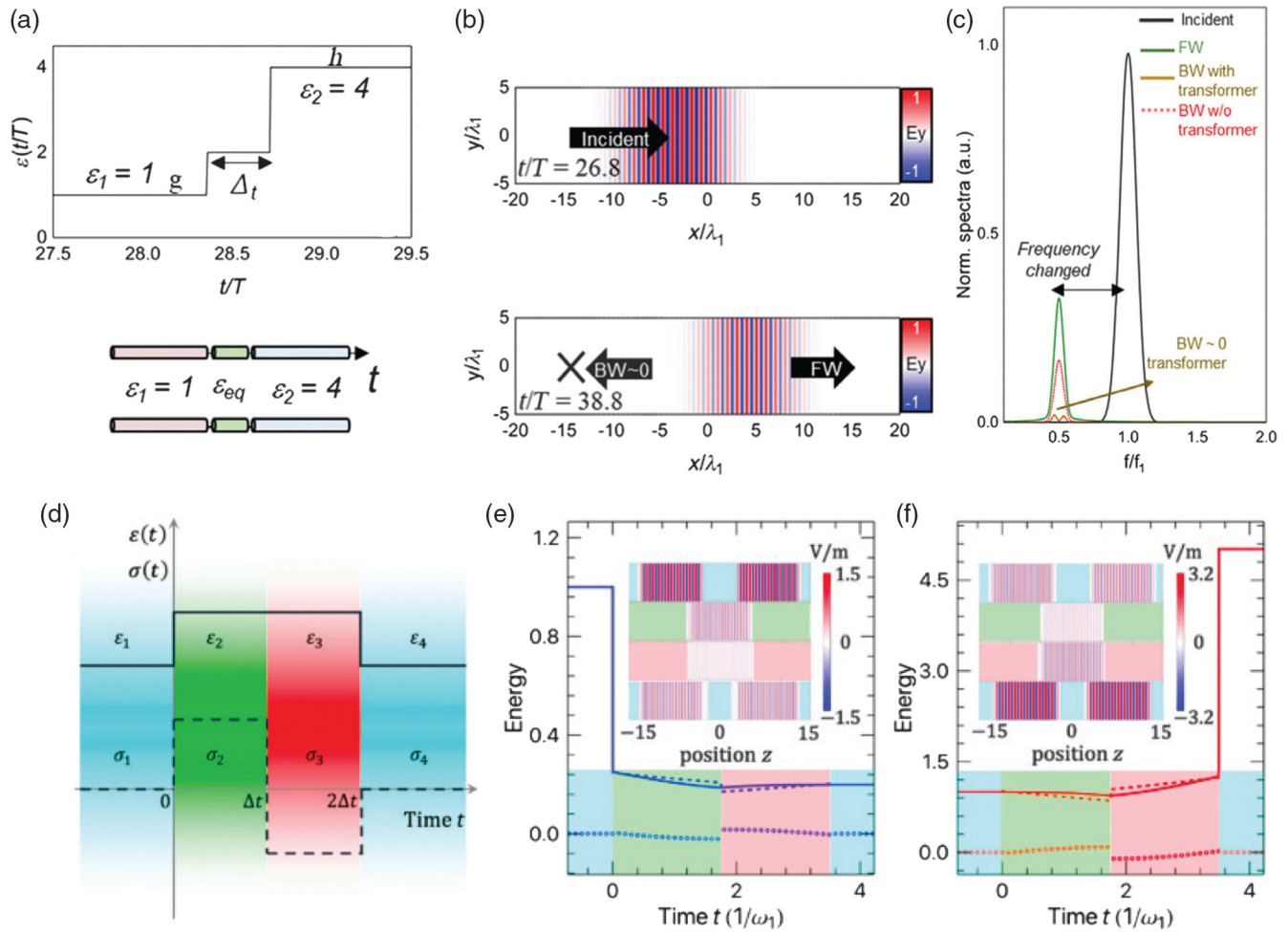
Fig. 2 (a) Schematic of the antireflection temporal coatings proposed in Ref. 39. (b) Numerical results for the field distribution before and after the temporal scattering, showing the incident and transmitted waves, with minimized reflection due to the temporal coating shown in (a). (c) Spectra of the incident, forward, and backward waves. (d) Schematic of TPT symmetric structures proposed in Ref. 40. (e) and (f) The time evolution of the normalized energy (solid curves) and its two constitutions (circle symbols for interferences and the dashed curves for another). (e) Maximum total power and (f) minimum total power. Insets are the field distributions in simulations before, during, and after the TPT slabs. Figures adapted from Refs. 39 and 40.

temporal interfaces. Although Eq. (8) looks similar to the condition for impedance matching in the spatial case,[41] it is more than a dual to its spatial counterpart. First, the frequency is shifted from f_1 to $f_2 = \sqrt{\varepsilon_1/\varepsilon_2} f_1$, as shown in Fig. 2(c). In addition, the energy and power flow of the waves have also been modified as we change the permittivity of the material.

More recently, it has been shown that extreme power and energy manipulation can be achieved in these types of temporal slabs once loss and gain are considered. In analogy to conventional parity-time (PT) symmetry with balanced gain and loss,[42] Li et al.[40] investigated a scenario where a pair of temporal slabs obey temporal parity-time (TPT) symmetry. In their work, the temporal parity operation flips the arrow of time, whereas the "time" operation is defined to reverse the waves in space. TPT-symmetric temporal slabs are therefore realized if an unbounded medium is switched from a positive to a negative conductivity in time, $\sigma_2 = -\sigma_3 > 0$, for equal duration Δt before switching back to the initial Hermitian medium, as shown in

Fig. 2(d). Instantaneous material responses for both permittivity and conductivity have still been assumed here.

By introducing a general temporal scattering matrix formulation, which may be powerfully applied to any multilayer configuration of temporal interfaces, such (temporally finite) TPT-symmetric structures have been proven to always reside in their symmetric phase, for which the scattering matrix supports unimodular eigenvalues. Interestingly, the nonorthogonal nature of wave interference in non-Hermitian media enables exotic energy exchanges, despite the fact that the overall temporal bilayer is in its symmetric phase. As a result, the total power flow carried by the waves after the switching events, $P_{tot}(t) = P^+(t) + P^-(t)$ with $P^\pm(t)$ for the forward/ backward propagating wave, can be significantly different from the incident one. By controlling the relative phase of two incident counterpropagating waves, one can reach drastically different total power flows for the same TPT-symmetric temporal bilayer. As an example, for $n_1 = 1$, $n_2 = 2 - j0.2$, and

$2\omega_1 \Delta t = 3.5$, the temporal evolution of the normalized stored energy density (solid curves) and its two components $U_i = 2\varepsilon[|E^+(t)|^2 + |E^-(t)|^2]$ [dashed curves, proportional to the total power flow in the two waves $E^+(t)$ and $E^-(t)$, and equal to the total stored energy in Hermitian media] and $U_c = 2\operatorname{Re}[n(n^* - n)E^+(t)E^-(t)^*]$ (circle symbols, stemming from the nonorthogonality of the counterpropagating waves in non-Hermitian media) are shown in Figs. 2(e) and 2(f) for two different relative phases of the input waves, yielding widely different power flows after the switching events. Thus, dramatic power amplification and attenuation can be achieved in such non-Hermitian temporal bilayers as a function of the relative phase of the excitations, as a dual phenomenon to laser-absorber pairs in conventional PT-symmetric systems.

2.3 Temporal Switching in Anisotropic Media

Recent research has added new degrees of freedom to enable exotic wave transformations based on time-switching. One intriguing possibility is to consider material anisotropy. In 2018, Akbarzadeh et al.[28] raised the question of whether it is possible to realize an analog of Newton's prism, shown in Fig. 3(a), in a time metamaterial. To map spatial frequencies into temporal frequencies, not only temporal invariance needs to be violated but also spatial symmetry breaking is required to bridge different momenta with different frequency channels, as shown in Fig. 3(b). The result is an inverse prism, as shown in Fig. 3(c), in which an unbounded isotropic medium with scalar refractive index n_1 is switched to a uniaxial medium with $\bar{\bar{n}}_2 = \operatorname{diag}(n_\parallel, n_\parallel, n_\perp)$ at $t = t_0$. The right part of Fig. 3(c) represents
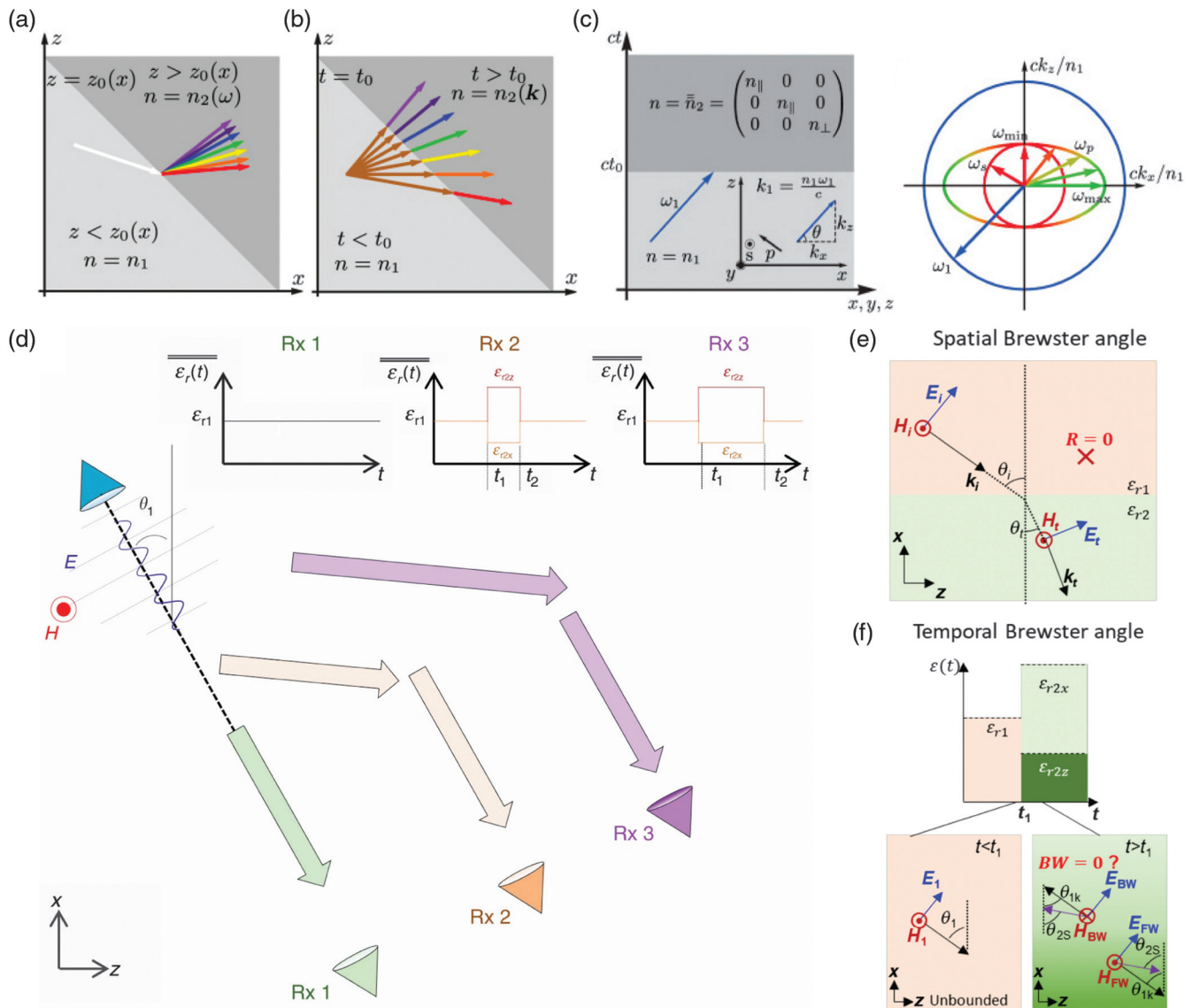

Fig. 3 (a) A conventional prism decomposing white light into its frequency components in different directions. (b) An inverse prism that maps the light with different momentum into different frequencies. (c) Implementation of the inverse prism proposed in Ref. 28. (d) Temporal aiming proposed in Ref. 43. (e) The conventional Brewster angle. (f) Temporal Brewster angle described in Ref. 44. Figures adapted with permission from Refs. 28, 43, and 44.

the isofrequency curves of the medium before and after switching. Because the medium remains homogeneous, the conservation of the wavenumber k (momentum) still holds, leading to "birefringence" at temporal frequencies. A monochromatic wave at frequency ω_1 propagating in the isotropic medium before switching will then be mapped to different frequencies, depending on its polarization and momentum, following:

$$n_1\omega_1 = \pm n(k) = \begin{cases} \pm n_\parallel \omega_2 & s\text{-polarization} \\ \dfrac{\pm n_\parallel n_\perp \omega_2}{\sqrt{n_\parallel^2 \cos^2\theta + n_\perp^2 \sin^2\theta}} & p\text{-polarization} \end{cases}, \quad (9)$$

with $\theta = \arctan(k_z/k_x)$ as defined in Fig. 3(c). In general, linearly polarized light experiencing such an inverse prism will feature Lissajous polarization with a time-varying phase difference between two orthogonal field components, due to the distinct values of ω_2 for s- and p-polarizations.

One interesting phenomenon for wave propagation in anisotropic crystals is that the group velocity does not necessarily align with the phase velocity.[10] Based on this feature, the concept of temporal aiming was proposed in Ref. 43. Figure 3(d) shows an overview of this phenomenon based on isotropic-to-anisotropic switching. A p-polarized wave packet is immersed in a time-switched medium. Different switching schemes $\bar{\bar{\varepsilon}}_r(t)$ shown in the insets would route the signal to different receivers [denoted Rx 1 to 3 in Fig. 3(d)]. For an incoming wave with propagation angle $\theta_1 = \tan^{-1}(k_z/k_x)$, the direction of the momentum k after switching to the anisotropic medium remains the same $\theta_{2k} = \theta_{1k} = \theta_1$, while that of the Poynting vector $\mathbf{S}$ is redirected to

$$\theta_{2S} = \arctan\left(\frac{\varepsilon_{r2z}}{\varepsilon_{r2x}} \tan\theta_1\right), \quad (10)$$

assuming that the anisotropic medium is a uniaxial crystal with $\bar{\bar{\varepsilon}}_{2r} = \text{diag}(\varepsilon_{2x}, \varepsilon_{2x}, \varepsilon_{2z})$. The discrepancy between θ_{2S} and θ_1 plays a key role in the aiming process by enforcing that the wave packet drifts transversely to the initial propagation direction. After an appropriate duration, the medium is then switched back to the initial state to allow the signal to travel again at the same frequency and direction. The idea of signal aiming through temporal switching paves the way to routing waves through temporal interfaces, creating a form of temporal waveguiding.

Another interesting phenomenon exploiting temporal switching with anisotropic media is the temporal Brewster angle.[44] The conventional Brewster angle is defined as the angle at which the reflection of the p-polarized incidence vanishes, as shown in Fig. 3(e). Its temporal counterpart is shown in Fig. 3(f) and similarly determined by the condition that no backward wave is produced at the time interface. The temporal Brewster angle is given by the following simple expression:

$$\theta_{tB} = \arcsin\sqrt{\frac{\varepsilon_{r2x}(\varepsilon_{r2z} - \varepsilon_{r1})}{\varepsilon_{r1}(\varepsilon_{r2z} - \varepsilon_{r2x})}}. \quad (11)$$

Notice that the Brewster angle for s-polarized waves is also expected if we consider biaxial anisotropy where $\varepsilon_{2x} \neq \varepsilon_{2y} \neq \varepsilon_{2z}$. These results open new avenues in controlling the polarization of waves by exploiting temporal interfaces. For instance, Xu et al.[45] reported complete polarization conversion using anisotropic temporal slabs.

2.4 Temporal Switching in the Presence of Material Dispersion

All previous results have assumed that the materials involved are nondispersive, such that they respond to abrupt switching events instantaneously. However, caution is needed about this assumption, as the material response may have temporal dynamics comparable with the finite switching times of realistic modulation processes. In general, the temporal non-local response (dispersion) of a material can be considered by assuming a susceptibility kernel in the form $\mathbf{D}(t) = \varepsilon_0[\varepsilon_\infty \mathbf{E}(t) + \int dt' \chi(t, t')\mathbf{E}(t - t')]$, where ε_∞ is the background relative permittivity and $\chi(t, t')$ is the time-dependent electric susceptibility, which must satisfy causality. Recently, the generalization of the Kramers–Kronig relations has been introduced for both adiabatic[46] and nonadiabatic[47] time-varying susceptibilities χ. Research on temporal switching with material dispersion dates back to Fante's and Felson's work in the 1970s.[20,21] In parallel, wave propagation phenomena such as self-phase modulation and frequency conversion were studied in rapidly growing plasmas due to ionization.[48–51] Comprehensive reviews on time-varying plasmas can be found in Refs. 17 and 27.

Once material dispersion is not negligible, it has been shown that the electric field $\mathbf{E}$ becomes continuous at a time interface, giving rise to additional temporal boundary conditions in addition to Eq. (3). The temporal boundary conditions in this scenario have been derived in Ref. 30 from the perspective of Parseval's theorem and in Ref. 31 based on the balance of distributions. In the time domain, a Drude–Lorentz medium features a second-order differential equation for the electric polarization density $\mathbf{P}$:

$$\frac{d^2\mathbf{P}}{dt^2} + \gamma\frac{d\mathbf{P}}{dt} + \omega_0^2\mathbf{P} = \varepsilon_0\omega_p^2\mathbf{E}, \quad (12)$$

where γ is the collision damping rate, ω_0 is the natural frequency of the free electron gas, and $\omega_p = \sqrt{Ne^2/(m_e\varepsilon_0)}$ with the volumetric carrier density N, and the electron's mass m_e, and charge e. A time-switched N was considered in Refs. 29 and 30 to effectively change ω_p abruptly. The boundary conditions at the temporal interface turn out to be the continuity of $\mathbf{B}$, $\mathbf{D}$, $\mathbf{E}$ (and therefore $\mathbf{P}$) and $d\mathbf{P}/dt$. The additional degrees of freedom thereby introduced can give rise to a total of four (distinct or degenerate) solutions for the new eigenfrequencies $\pm\omega_{1,2}$.

2.5 Time Interfaces in Spatial Structures

While drawing significant attention, the concept of time-switching still bears the question about accessibility to practical implementations. Until now, the experimental work demonstrating time-reversal at a temporal interface has been limited to water-wave phenomena by Fink's group, whereby a water tank was uniformly shaken by an impulse, leading to the refocusing of the waves back to their emission point.[52] In addition to limitations in the achievable modulation speed and strength, one chief difficulty also lies in altering a medium in its entirety to conserve momentum in all directions. Huge energy exchanges and stringent simultaneity of switching are typically required. Instead, more and more effort has been geared toward switching materials only for spatially finite structures or in lower dimensions. For instance, temporal reflections were

studied in Refs. 53 to 55 for two-dimensional (2D) graphene plasmons, as shown in Fig. 4(a). In one-dimensional (1D) transmission lines, broadband and efficient impedance matching can be achieved by time-switching, as shown in Fig. 4 from Ref. 56. Since time-switching relaxes the constraint of time-invariance, the proposed matching schemes can go beyond the conventional Bode–Fano efficiency bounds.

Taking advantage of enhanced light–matter interactions in finite structures that support resonances, we can extend temporal switching to other applications. Switching resonant cavities enables possibilities for plasma radiation[61] and photon generation.[62] Similar ideas have also been applied to induce static-to-dynamic field radiation in a switched dielectric brick sandwiched in a waveguide.[63] Li and Alù explored a time-switched Dallenbach screen, whose schematic is shown in Fig. 4(c), showing that time-switching can extend the absorption bandwidth by changing the permittivity of an absorber while a broadband signal enters it.[57] On a related note, Mazor et al. unveiled how an excitation can be unitarily transferred between coupled cavities by switching the coupling strength, even if the detuning between the cavities is large.[58] An example of this phenomenon in a coupled LC resonator pair is shown in Fig. 4(d); by properly switching the value of the coupling admittance, the energy stored in the LC resonator on the left can be transferred to the one on the right efficiently, with robustness

to large detuning between the two resonance frequencies. Subwavelength time-modulated meta-atoms have also been explored by Tretyakov's and Fleury's groups,[64] developing a consistent description of the interplay between time-modulation and dispersive polarizability,[65,66] whereas Engheta's group recently extended this concept to anisotropic meta-atoms, using it to demonstrate temporal wave deflection,[59] as shown in Fig. 4(e).

Finally, abrupt changes to the structural dispersion of a cavity, realized, e.g., by switching part of a structure, constitute yet another intriguing degree of freedom to be exploited. For instance, in Ref. 60, Miyamaru et al. achieved ultrafast terahertz frequency shifts by metalizing the upper boundary of a single-metalized waveguide at subpicosecond timescales via photocarrier excitation, thereby modifying its dispersion relation and inducing a large frequency shift, as shown in Figs. 4(f) and 4(g). Similarly, nonlinear terahertz generation was reported later in ultrafast time-varying metasurfaces.[67] Abruptly altering a spatial boundary can be interpreted heuristically as switching the effective permittivity of the waveguide structure,[68] which also enforces a temporal interface on the fields inside the waveguide.

To summarize, in this section, we discussed fundamental aspects of the electromagnetics of time interfaces: we revisited the temporal boundary conditions for Maxwell's equations and highlighted a few representative works on temporal scattering and interference. Further theoretical opportunities include the
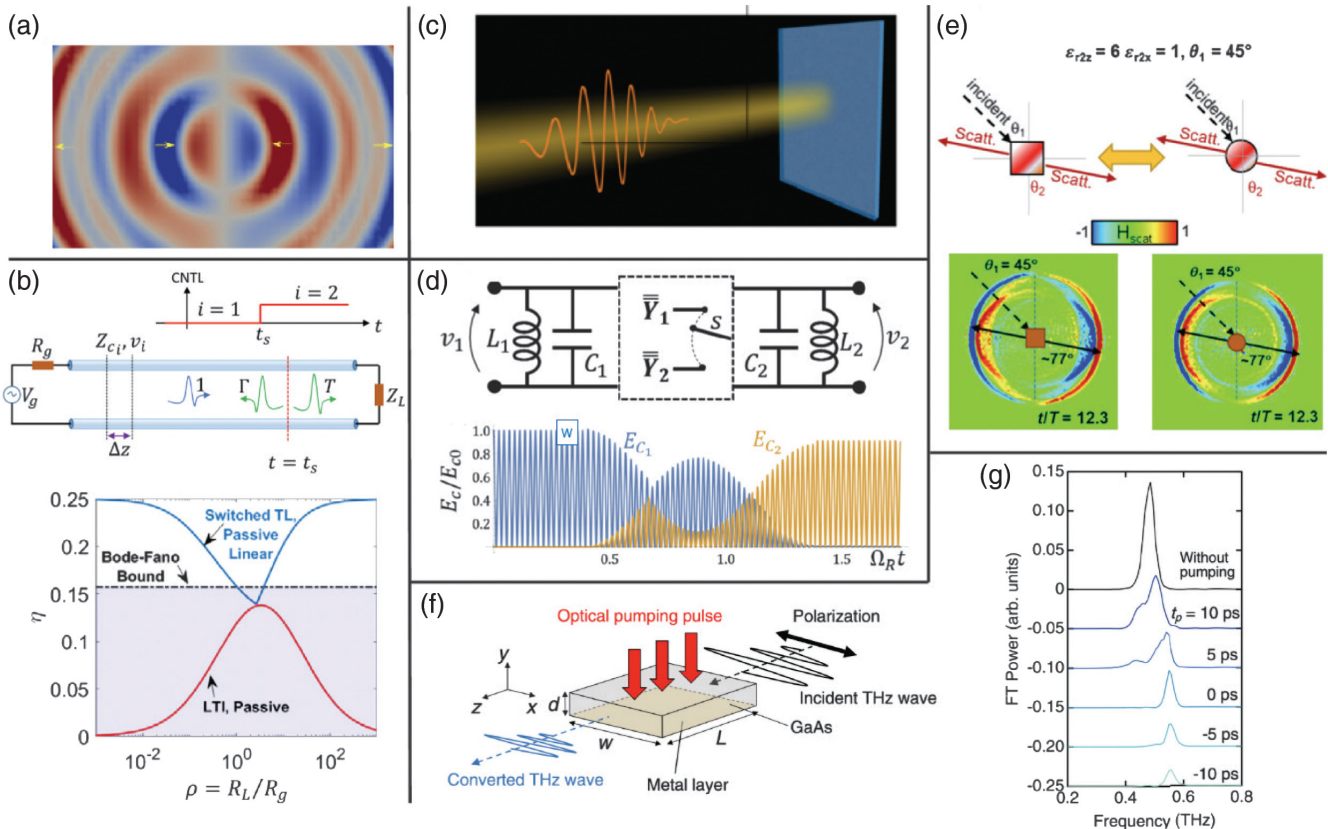

Fig. 4 (a) Temporal reflection of graphene plasmons reported in Ref. 54. (b) Impedance matching using a time-switched transmission line.[56] (c) Time-switched thin absorber in Ref. 57. (d) Unitary excitation transfer between two coupled circuit resonators.[58] (e) Temporal deflection caused by isotropic-to-anisotropic switching on meta-atoms.[59] (f) Temporal switching of structural dispersion for ultrafast frequency-shifts, proposed in Ref. 60. (g) Corresponding frequency spectra for the switching in (f). Figures adapted from Refs. 54, 56, 57, 58, 59, and 60.

study of more sophisticated material models, such as non-Hermitian, anisotropic, and even bianisotropic switching mechanisms, also in spatially structured systems. In the quest for extreme wave phenomena, temporal switching with exotic media has opened a brand-new avenue for electromagnetics research and beyond, although its ultimate impact will hinge upon further implementations of temporal switching experiments, some of which we will discuss in Sec. 5. In the next section, we make use of the building blocks of temporal switching discussed here to construct (quasi-)periodic temporal structures and investigate some of the numerous opportunities that stem from more complex time-varying systems.

3 Photonic Time-Crystals

The simplest mechanical archetype of a periodic time-modulated wave system is a pendulum, whose length is periodically modulated in time, one historic example being the "Botafumeiro," an 80 kg incensory at the Cathedral of Santiago de Compostela, whose chain is periodically pulled up and down via a pulley by monks, reaching speeds of 68 km/h over arc lengths of 65 m within 17 modulation cycles[69] (a more familiar one is the child swing, whereby the height of the center of mass is modulated). In fact, a characteristic feature of this gain effect (called parametric amplification) is its exponential growth rate, as opposed to the linear growth that occurs in a driven oscillator.

We can make use of the scattering coefficients derived in Sec. 2 to construct the building blocks of parametric amplification in electromagnetism. After a first time-switching leading to a change of impedance $Z_1 = \sqrt{\mu_1/\varepsilon_1} \to Z_2 = \sqrt{\mu_2/\varepsilon_2}$, the displacement field at time t will comprise forward and backward waves according to: $D_2(t) \propto T_{12}e^{j\omega_2 t} + R_{12}e^{-j\omega_1 t}$. If we now switch the material again after a time Δt_2, the new forward waves will encompass doubly reversed and doubly transmitted waves. Conversely, the backward waves will consist of waves which were reflected on only one of the two switching events, giving after an additional time Δt_3:

$$D_2/D_0 \propto (T_{12}e^{j\omega_2 \Delta t_2}T_{23} + R_{12}e^{-j\omega_2 \Delta t_2}R_{23})e^{j\omega_3 \Delta t_3}$$
$$+ (T_{12}e^{j\omega_2 \Delta t_2}R_{23} + R_{12}e^{-j\omega_2 \Delta t_2}T_{23})e^{-j\omega_3 \Delta t_3}. \quad (13)$$

This argument can be easily extended for a given number of switching events, with forward and backward waves consisting of scattering contributions involving an even and odd number of time-reversal processes $R_{i,i+1}$, respectively.

To study in more detail the effect of a periodic modulation, let us set the final parameters in a double-switching process equal to the initial ones, $\varepsilon_3 = \varepsilon_1$ and $\mu_3 = \mu_1$, which forms one modulation cycle. Evaluating the energy content of the forward and backward waves, we arrive at

$$|\mathbb{T}_2|^2 = 1 + \frac{1}{2}\frac{(Z_1^2 - Z_2^2)^2}{Z_1^2 Z_2^2}\sin^2(\omega_2 \Delta t_2), \quad (14)$$

$$|\mathbb{R}_2|^2 = \frac{1}{2}\frac{(Z_1^2 - Z_2^2)^2}{Z_1^2 Z_2^2}\sin^2(\omega_2 \Delta t_2), \quad (15)$$

so that it is evident that the relation: $|\mathbb{T}_2|^2 = 1 + |\mathbb{R}_2|^2$ must always hold true regardless of the extent and duration of the "temporal slab." To demonstrate the generality of this argument for

any number of switchings, it is instructive to keep in mind here that momentum conservation must hold true across any number of such scattering processes. Calculating either the Abraham (kinetic) momentum $\mathbf{E} \times \mathbf{H}$ or the Minkowski (canonical) momentum, $\mathbf{D} \times \mathbf{B}$ must in fact yield the same total final momentum. As a result, it should not come as a surprise that any amplification of forward waves must be accompanied by an equal amplification (or generation) of backward waves, so the overall effect of the parametric pumping is to effectively generate a standing wave on top of the incoming beam. Clearly, in a realistic scenario, since the forward and backward waves are orthogonal in the absence of modulation, they can be independently outcoupled, leading to a net increase of energy in both forward and backward waves. As another consequence of momentum conservation, the energy in the system cannot be reduced: any change in the forward wave amplitude must be compensated by the generation of a backward wave, which can only have a positive contribution to the total energy in the system. Notice how this is dual to the spatial case, where the total energy in the system must be conserved, so the power in the forward-scattered waves can only be reduced by a scattering process. Finally, it is worth pointing out that no energy exchange can occur from time-switching if the system is impedance-matched. As we will discuss in Sec. 4, however, it is still possible to have gain in impedance-matched scenarios within certain spatiotemporal modulation regimes (Sec. 4.3).

With these dualities in mind, we are now ready to study the key features of infinite time-periodic (and quasiperiodic) systems, which we refer to here as PTCs, although it should be noted that this term bears a slight ambiguity with the concept of time-crystal in condensed matter physics,[70,71] where it denotes a stable phase of matter that spontaneously breaks continuous time-translation symmetry. Here, we intend PTCs as active systems relying on an externally induced modulation of their constitutive parameters, and whose underlying pumping mechanism is unaffected by the linear wave dynamics imparted onto a probe wave.

In a conventional photonic space-crystal (PSC), it is well known that Bragg scattering between waves separated in momentum by integer multiples of a reciprocal lattice vector $\mathbf{g}$ of the crystal leads to the formation of bandgaps in energy, in correspondence with the high-symmetry points in reciprocal space (in 1D, this would happen at $k = 0, \pm g/2$). In these gaps, the states have an imaginary momentum component, thus decaying into the crystal (growing states are forbidden by energy conservation). It is expected, therefore, that modulating a system periodically in time at frequency Ω will yield bandgaps in momentum (k-gaps) near the frequency $\Omega/2$, where Ω plays the role of a reciprocal lattice vector, as a result of the interference between the waves that are forward-scattered by the modulation, and those that are time-reversed. However, while in a PSC, the wavevector is imaginary inside the bandgap; in a PTC it is the energy that acquires an imaginary component within a k-gap. As expected from our previous discussion on momentum and energy conservation, while waves must spatially decay into the PSC to preserve energy, they can only grow in time as they interact with a PTC, to preserve momentum. This duality is shown in Figs. 5(a) and 5(b). Let us consider an infinite series of switching events between ε_1 and ε_2, as shown for a few cycles in Fig. 5(b). Since the problem is periodic, the Floquet (Bloch) theorem holds, so the solution may be written as $\psi(t) = e^{i\Omega t}\phi(t)$, where $\phi(t) = \phi(t + T)$ and $T = 2\pi/\Omega$ is the period of the modulation. For the specific case of a step-
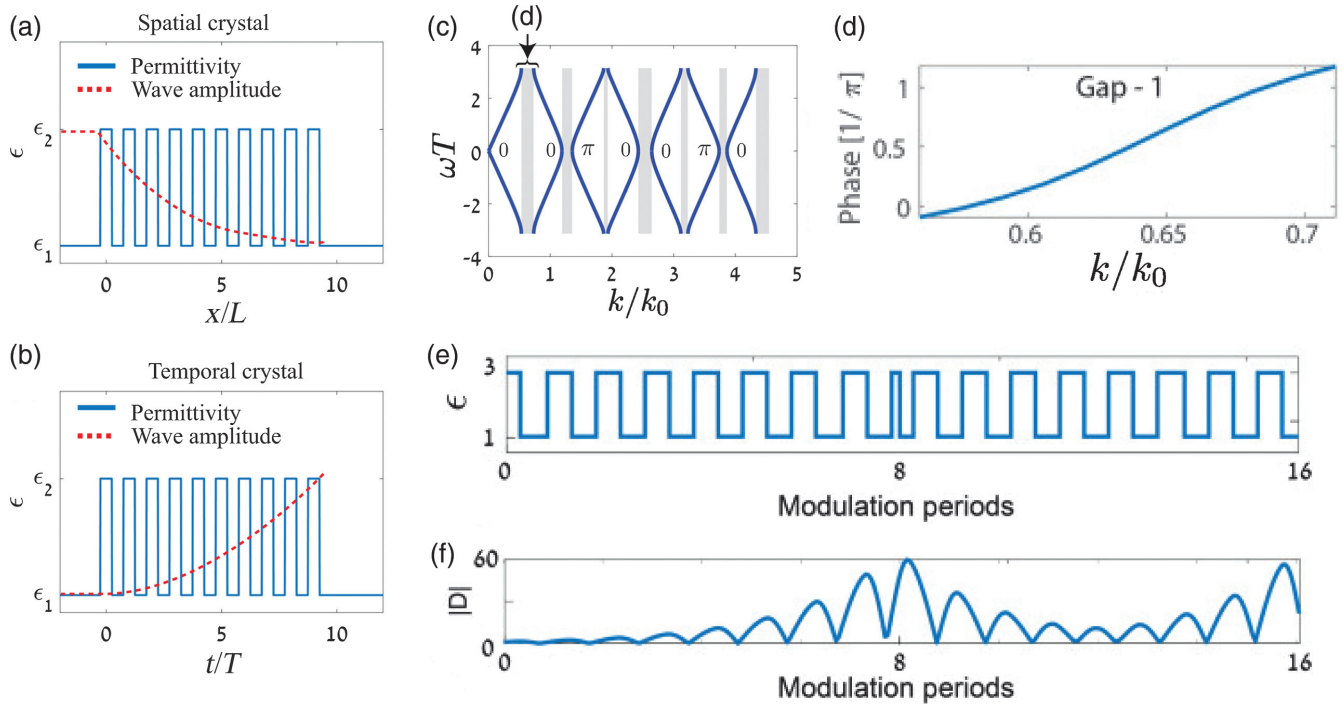
Fig. 5 (a), (b) Example of a (finite) layered (a) PSC and (b) PTC, and corresponding wave behaviour within the respective band gaps. (c) Band structure of a PTC, showing k-gaps and Zak numbers of the different bands. (d) Change of Zak phase across the first k-gap. (e) Example of an edge between two PTCs with opposite Zak phase. (f) Numerical demonstration of the effect of a temporal edge between two topologically inequivalent PTCs: the parametric amplification process is interrupted and the wave amplitude is depleted for a few periods following the temporal edge, forming a temporally localized state. Figures adapted from Ref. 72.

like modulation, the temporal scattering coefficients can be related to each other by exploiting the symmetry $T_{12} + R_{12} = T_{21} + R_{21} = 1$, so the Floquet bands [shown in Fig. 5(c)] can be calculated analytically.[72] Notice how the k-gaps hosting the amplifying states open at $\omega = \Omega/2$ (i.e., $\omega T = \pi$, where T is the modulation period). The reason for this can be read off the solution for the double-switching problem in Eq. (14–15). Notice how the time-interval Δt_2 between the two switching events determines whether or not gain will occur: if this interval, which corresponds to half of a modulation period T, is a quarter of the wave period (i.e. $\Delta t_2 = \pi/(2\omega_2)$), so that $\Omega = 2\pi/T = 2\omega_2$, then at each switching process a net energy input from the contribution of the sinusoidal term in Eq. (14) will be coherently fed into the waves, leading to exponential growth or, in the presence of dominant losses, loss-compensation.[73] Related ideas were recently investigated, such as "multi-layer" temporal slabs to design temporal transfer functions, in analogy with multilayer matching filters in spatial transmission line theory,[74,75] while the effects of modulating both dielectric and magnetic parameters in a PTC were studied in Ref. 76.

3.1 Topology in Photonic Time-Crystals

One recent direction emerged in the context of spatial crystals is that of topologically nontrivial photonic phases and symmetry-protected edge modes found at their interface with a topologically inequivalent crystal. The natural question of whether such a framework exists for temporal crystals has recently been answered in the affirmative, although experimental

observations of temporal topological edge states are still missing.[72] In 1D (infinite) crystals, the topological character of the system is quantified via the Zak phase. A temporal edge state must therefore lie at the temporal interface between PTCs characterized by different Zak phases. For a layered PTC, the Zak phase can be calculated analytically via Floquet theory, and its change across the first k-gap is shown in Fig. 5(d).[72] Far from a trivial generalization, however, a temporal edge is a markedly different object than a spatial one. The edge modes commonly found at the interface between topologically inequivalent crystals are now to be sought near (more specifically later than) a specific instant of time, at which the properties of the PTC are suddenly changed. In addition, while spatial edge states occur within the frequency gap of a material where the eigenstates of the infinite crystal are evanescent, temporal edge states in a PTC are only found within k-gaps, so the underlying wave dynamics is parametric amplification, and the transient wave that constitutes the edge state has the effect of temporarily opposing the exponential growth, as shown in Figs. 5(e) and 5(f).[72]

In spite of time being a 1D quantity, time-modulation can also provide a pathway toward higher-dimensional topological effects. This can be accomplished by constructing synthetic frequency dimensions, using the frequency spectrum of the modes supported by a structure as an effective lattice of states, in analogy with the sites of a tight-binding lattice, as shown in Figs. 6(a)–6(c). Similarly to electrons in a simple 1D lattice, photons in, e.g., a periodically modulated ring resonator may be described by a tight-binding Hamiltonian
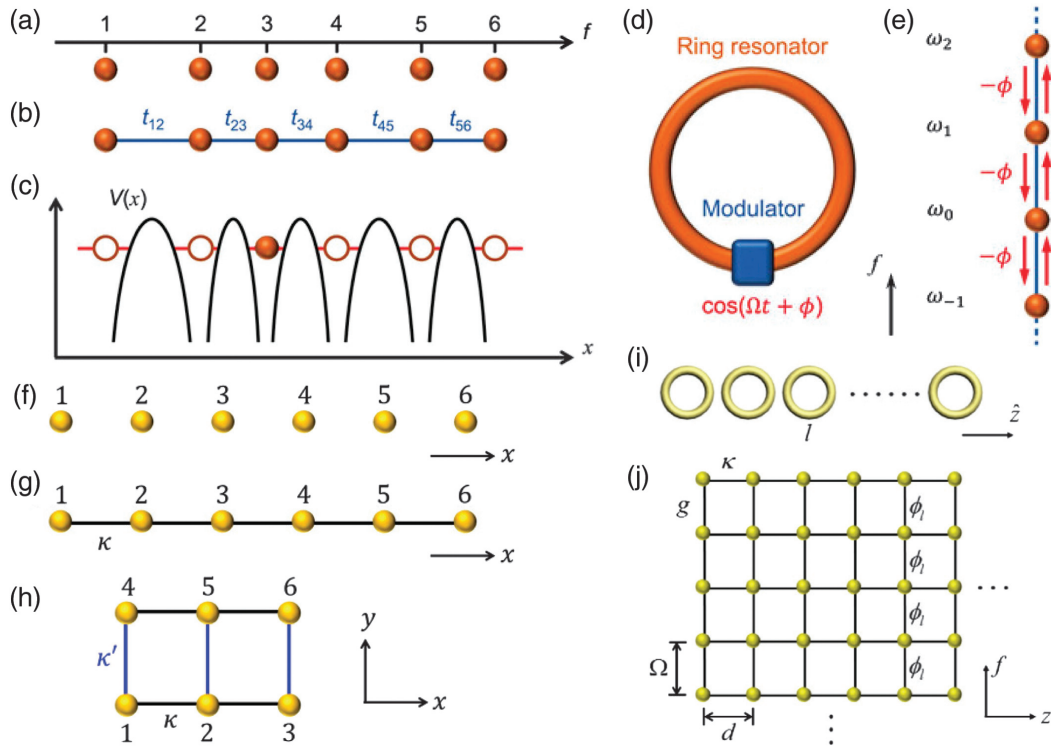
Fig. 6 (a) The resonant modes of a structure form a lattice in the frequency dimension. (b) Hopping through its sites can be enabled by time modulation, which can couple their different frequencies. (c) The resulting Hamiltonian is analogous to that of electrons in a periodic ionic potential. (d) A ring resonator combined with a modulator can reproduce such a model, (e) enabling hopping between its equally spaced resonant modes.[77] (f)–(h) A synthetic dimension may be constructed in a tight-binding model by introducing long-term coupling between the elements of a chain. In the time-domain, this can be realized by modulating the system at multiple frequencies.[78] (i), (j) A spatially 1D chain of ring resonators can be combined with temporal modulation to form a synthetic 2D lattice.[79] Figures adapted from Refs. 77–79.

$$H_1 = g \sum_m (a^\dagger_{m+1} a_m e^{i\phi} + a^\dagger_m a_{m+1} e^{-i\phi}), \tag{16}$$

where $a^\dagger_m$ and a_m are the photon creation and annihilation operators for the m'th mode on the lattice, $g = \kappa\Omega/2\pi$ is the hopping amplitude, κ is the modulation strength, Ω is the modulation frequency, and ϕ is the modulation phase.[77] In fact, just as electrons hop between sites of a lattice, a dynamical modulation can make photons hop between different modes of the resonator, as long as the modulation frequency is similar to the difference $\Omega_R = 2\pi v_g/L$ between the modes of the structure, where v_g and L are the group velocity of the waveguide constituting the resonator and L is its length. The simplest instance of such a lattice may be realized with a single ring resonator combined with a periodic modulator, shown schematically in Fig. 6.

Importantly, such a ladder does not need to be unidimensional; additional dimensions may be constructed from any degree of freedom by simply introducing additional coupling terms between a lattice of resonators, or, in a synthetic frequency dimension, between modes,[79] which means that a linear lattice can now be equivalently described as a folded one to highlight its higher dimensionality, as shown in Figs. 6(f)–6(h). With time-modulation, this can be done by considering two periodic modulations of different frequencies, e.g., $\Omega_1 = \Omega_R$

and $\Omega_N = N\Omega_R$, thus introducing coupling between N'th-neighboring modes in the lattice, so the Hamiltonian above can be generalized to

$$H_N = g \sum_m (a^\dagger_{m+1} a_m e^{i\phi} + \text{h.c.}) + g_N \sum_m (a^\dagger_{m+N} a_m e^{i\phi_N} + \text{h.c.}), \tag{17}$$

where $g_N = \kappa_N \Omega_R/2\pi$. Here, the second term accounts for the coupling between modes separated by a frequency gap $N\Omega_R$, and it is mathematically equivalent to the addition of a second dimension. Time-modulation can also be combined with other degrees of freedom, such as orbital angular momentum[80] or spatial lattices[79] to implement a range of photonic effects, from nontrivial Chern numbers to effective gauge fields and spin-momentum locking. Implementations of synthetic frequency dimensions have been realized in RF with varactors[81] and superconducting resonators,[82] and in the near-infrared with fiber and on-chip electro-optic modulators,[83,84] as well as all-optically via four-wave mixing, with frequency spacings generally ranging from MHz to THz.[77] A recent proposal makes use of a single ring-resonator coupled to an array of optomechanical pumps and a single electro-optic modulator to realize an on-chip 2D topological insulator with two synthetic dimensions.[85]

3.2 Non-Hermitian and Disordered Photonic Time-Crystals

Another promising direction for new opportunities in wave manipulation is the interplay between temporal structure and Hermiticity. Gain in electromagnetism has conventionally been associated with the use of active media, providing wave amplification in the form of a negative dissipation rate. However, as discussed above, time-modulation offers an alternative route toward gain. A complete analogy between non-Hermitian gain/loss and parametric processes cannot be drawn: in fact, it is evident from our previous discussion that a mere time-modulation cannot provide loss, as a consequence of momentum conservation, whereas an imaginary component in the response parameters of a medium can be used to provide either gain or dissipation depending on its sign.

This distinction between parametric and non-Hermitian gain makes it natural to ask what more can be achieved by modulating in time the non-Hermitian component of the material response. As discussed in Sec. 2, the switching of dissipation not only impacts the amplitude of a wave but also its phase and can also generate backward waves, leading to highly non-trivial temporal wave scattering. In one instance, it was recently shown that non-Hermitian time-modulation can be used for nonreciprocal mode-steering and gain in frequency space.[86] Consider the setup shown in Fig. 7(a): two resonators with mode-lifetimes γ_1 and γ_2 are coupled via a time-dependent coupling constant $k_0 + \Delta k' \cos(\Omega t) + j \Delta k'' \sin(\Omega t)$, resulting in a non-Hermitian time-Floquet Hamiltonian. Normally, a periodic modulation of the system enables similar upconversion and downconversion between modes of a structure. However, it was shown that the inclusion of a non-Hermitian component in the time-modulation of the coupling constant between the resonators can hijack such mode coupling, rerouting all of the energy into one of the two resonators, thus producing nonreciprocal gain.[86]

The link between time-modulation and PT symmetric Hamiltonians has also been discussed in some depth for the parametric resonance case, where the frequency of the modulation doubles that of the incoming light.[88] Elegantly, PT
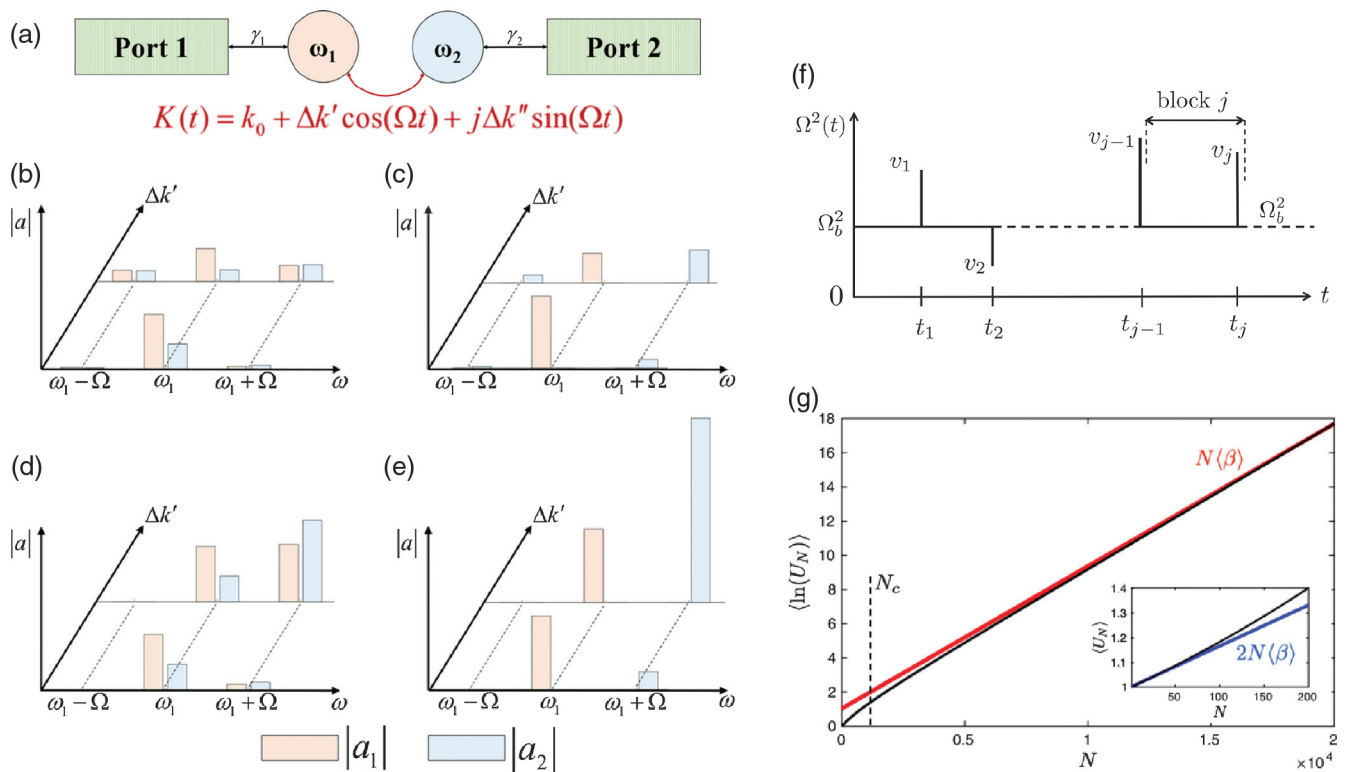

Fig. 7 (a) Two resonators coupled via a combination of constant (k_0), time-dependent Hermitian ($\Delta k'$), and time-dependent non-Hermitian ($\Delta k''$) coupling terms. (b)–(e) Wave amplitude under excitation via port 1 in the two resonators (orange and blue) for two arbitrary values of $\Delta k'$ at the excitation frequency (ω_1) and the two sidebands for (b) $k_0 \neq 0$ and $\Delta k'' = 0$ (energy stored in both sidebands and both resonators); (c) $\Delta k'' = 0$ and $k_0 = 0$ (energy channeled to sideband frequencies is all in the second resonator while the first only hosts the input frequency); (d) $\Delta k' = \Delta k''$ and $k_0 \neq 0$ (energy gained is nonreciprocally channeled into the upper sideband and it is distributed over both resonators); (e) $\Delta k' = \Delta k''$ and $k_0 = 0$ (energy gained is nonreciprocally channeled only into the upper sideband and uniquely in the second resonator).[86] (f) A random sequence of temporal δ-kicks results in (g) universal statistics observed by the energy in the system U. The energy at the N'th kick U_N is plotted against the step number N.[87] Figures adapted from Refs. 86 and 87.

symmetry breaking in these parametric systems can be related to the stability conditions of the Mathieu equation governing a harmonically modulated structure.[89] Such time-modulation-induced PT symmetric physics additionally enables not only lasing instabilities but also bidirectional invisibility due to anisotropic transmission resonance, when two PT-symmetric time-Floquet slabs are combined together such that their respective parametric oscillations cancel out exactly. New perspectives relating exceptional point physics and parametric modulation may be also found in Refs. [90] to [92], whereas Refs. [93] and [94] investigate topological phases in non-Hermitian Floquet photonic systems.

Another interesting direction for non-Hermitian time-modulated systems relates to the temporal analog of the causality relations of conventional passive media.[46] As a well-known consequence of causality, imposed by demanding that the response function of a system is only non-zero at times following an input signal, the real and imaginary parts of the response function of a system must relate to each other through the Kramers–Kronig relations. However, the spectral analog of these relations can also be constructed: if one would like the spectral response of a system to be uniquely non-zero for frequencies higher or lower than the input frequency, such that only upconversion or downconversion occurs, then there exist temporal Kramers–Kronig relations, which can provide a recipe for how the Hermitian and the non-Hermitian components of a time-modulation must be related in order for such asymmetric frequency conversion to occur. Related concepts have also been exploited for event-cloaking, broadband absorption, and synthetic frequency dimensions.[46,95]

The introduction of temporal disorder constitutes yet another avenue where the inequivalence between space and time may bear new perspectives in long-standing problems such as Anderson localization.[87,96–98] Interestingly, however, the conventional localization observed in spatially disordered media does not occur in a time-modulated system. Instead, in a similar fashion to the occurrence of edge states, the onset of the temporal analogue of Anderson localization manifests itself as an exponential growth in the energy of the waves. Such wave dynamics has been investigated both analytically,[87] demonstrating the universal statistics occurring in δ-kicked temporal media, and numerically,[97] as a disordered perturbation in a PTC. Experiments on wave dynamics in temporally disordered systems have also recently been performed with water waves.[96]

In the following section, we move on to briefly discuss temporally periodic surfaces, whereby the interplay of spatial discontinuities and temporal modulation can enable not only several realistic platforms for implementations with metasurfaces (which we delve further into in Secs. 4.4 and 5) but also completely new regimes of wave scattering.

3.3 Time-Modulated Surfaces

Amidst the rise of 2D materials, spatially structured surfaces, known as metasurfaces, have recently attracted enormous interest as the ultrathin counterpart of metamaterials. Periodically structured surfaces, or gratings, have however occupied a central role in photonics since its early days. In its interaction with waves in the far field, a 1D-grating can couple waves whose dispersion lives on the edge of the light cone by trading in-plane (k_x) and out-of-plane (k_z) momentum via both its in-plane structure and its transverse boundary,

such that they must add in quadrature to the total momentum $k_0 = \sqrt{\varepsilon}\omega/c_0$ of the impinging waves. Interestingly, time-modulated surfaces enable sharply different wave dynamics, due to the fact that the light cone treats the frequency axis on a different footing compared to the momentum axes; if we consider light impinging on a flat, time-modulated surface, its in-plane momentum k_x will now be conserved, whereas k_z and, importantly, the wave frequency ω are now allowed to change. Taking a vertical cut of the light cone for a fixed value of k_x, we see that the two quantities being traded by the surface, k_z and ω, must not add, but rather subtract in quadrature. As a result, the locus of points described by the available modes in the far field is no longer elliptical but hyperbolic. One consequence is that an increase in frequency caused by a temporal modulation corresponds to an increase in out-of-plane momentum and vice versa, the opposite of what happens between momentum components as they interact with a spatial grating.

One direction for time-modulated surfaces is the opportunity to couple radiation to surface waves in the absence of any surface structure. Since their dispersion curve lies outside of the light cone, surface waves are typically excited by breaking translational symmetry along the surface either via a localized near-field probe such as an SNOM tip[99] or periodically using a grating that induces a Wood anomaly.[100] However, the argument above can be exploited to envision surface-wave excitation via a temporal grating,[101] as shown in Figs. 8(d)–8(i). This approach brings the advantage of complete reconfigurability and use of higher-quality pristine materials, in particular in highly tunable 2D materials such as graphene and other van der Waals polaritonic materials, such as hexagonal boron nitride and MoO_3, thereby circumventing the very need for surface fabrication or near-field excitation techniques.

Another key technological application of time-modulated surfaces is frequency conversion.[103] The advent of metasurfaces across the electromagnetic spectrum has led to a surge of opportunities for advancing this known field of research both theoretically[104–112] and experimentally.[102,113–116] Recent implementations of frequency translation with metasurfaces have been recently carried out in the microwave regime,[102] and implementations with experimentally more practical discretized arrays of time- and space–time-modulated reactive elements are in steady development.[107,114] Several more experimental implementations are discussed in Sec. 5. Interestingly, the combination of bianisotropy and time-modulation has also been predicted to give rise to a nonreciprocal response (see Sec. 4.1).[117] Specific scattering studies have also been dedicated to periodically modulated slabs,[118] particularly in the context of parametric amplification.[112]

This recent surge of interest in time-modulated media has certainly highlighted the fundamental nature of the new wave phenomena that time-modulation can unlock, and it is evident that a wealth of research opportunities with PTCs, such as their implications in quantum systems and finite-size structures, still lies largely unexplored. Further directions involving space–time-modulated surfaces have nevertheless attracted remarkable interest already (Sec. 4.4). However, before discussing them, it is instructive to extend the theoretical background presented so far to the case of space–time modulations, which introduce a wealth of additional scattering phenomenology. At the end of Sec. 4, we combine these ideas on modulated surfaces with those of space–time media to study space–time metasurfaces (Sec. 4.4).
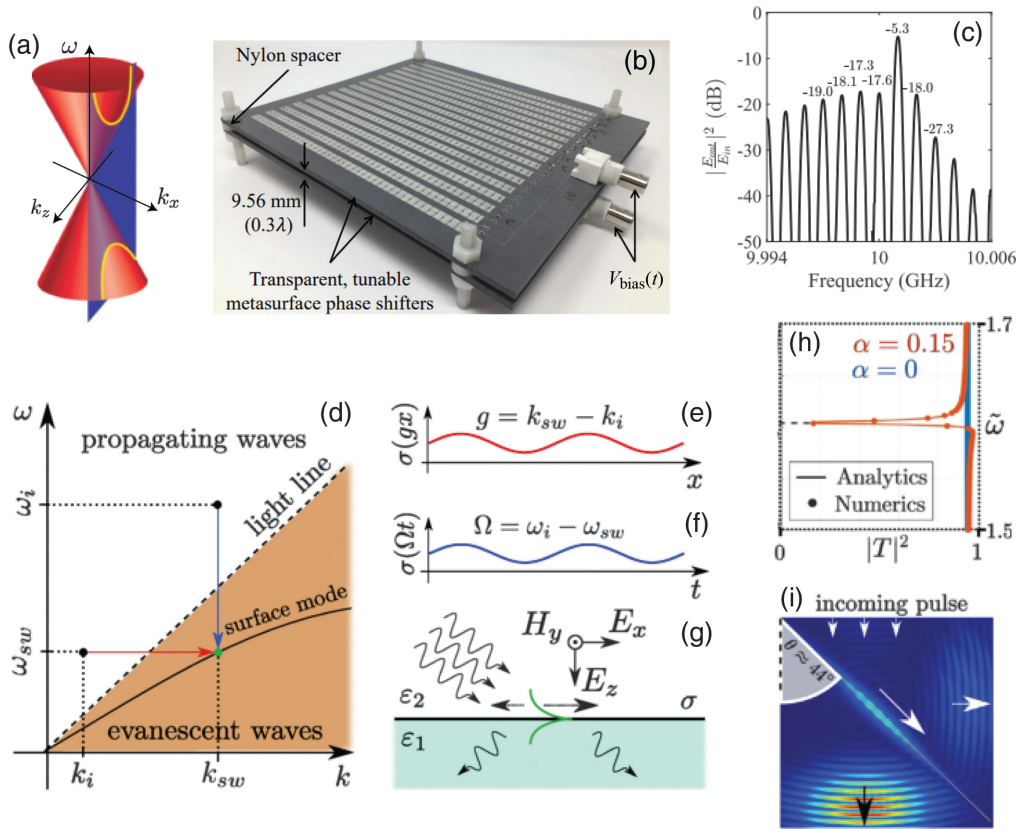
Fig. 8 (a) Light scattered from a flat, time-varying metasurface can access a locus of states that form a hyperbola in phase space, as opposed to an ellipse in spatial metasurfaces. (b) Implementation of a time-modulated metasurface at GHz frequencies. (c) A 1-MHz modulation performs efficient frequency conversion through time-modulation.[102] (d) Illustration of surface-wave excitation via the Wood anomalies using (e) spatial and (f) temporal modulation of (g) a surface. (h) Example of the Wood anomaly observed in transmission, the surface-wave excitation is explicitly shown in (i) from a finite-element-time-domain simulation.[101] Figures adapted from Refs. 102 and 101.

4 Spatiotemporal Metamaterials

Spatiotemporal modulations generally imprint a traveling-wave-like perturbation, of the form $\delta\varepsilon(x,t) = \delta\varepsilon(gx - \Omega t)$ (and similarly for μ) onto the response parameters of a medium, where $g = 2\pi/L$ and $\Omega = 2\pi/T$ are the spatial and temporal components of the reciprocal lattice vector associated with the spatial and temporal periods L and T of the modulation, which form a spatiotemporal lattice vector $p = (T, L)$, as shown in Figs. 9(a) and 9(b).[119] The idea of traveling-wave modulation has been in use since the early days of traveling-wave amplifiers, whereby electron beams are used to pump energy into copropagating microwave beams[122] and underwent a number of investigations in the 1960s[123–127] and later in the early 2000s.[128,129] Recently, the interest in these systems has revamped, with intense research efforts in the modeling and realization of space–time-modulated nonreciprocal systems (see Sec. 4.1).[25,121,130–134] In space–time media, neither frequency nor momentum is individually conserved, but rather a spatiotemporal Bloch vector (ω, k) forms a good quantum number, and the fields can generally be expressed as a superposition of a discrete set of Floquet–Bloch modes characterized by frequency-momentum vectors $(k + ng, \omega + n\Omega)$, where $n \in \mathbb{Z}$ as shown in Figs. 9(c)–9(f), so an eigenmode will have the form

$$\psi(x, t) = e^{j(\omega t - kx)}\sum_n a_n e^{jn(\Omega t - gx)}, \tag{18}$$

and an eigenvalue problem may be set in terms of either $\omega(k)$ or $k(\omega)$. Importantly, these new reciprocal lattice vectors (g, Ω) are not generally horizontal as in a PSC [Fig. 9(c)], nor vertical as in a PTC [Fig. 9(f)], but may form an arbitrary angle in the $\omega - k$ space, which may be smaller than the slope c_0 of the bands for the background medium (subluminal) [Fig. 9(d)] or larger (superluminal) [Fig. 9(e)], reducing to a pure temporal modulation in the limit where the modulation speed $v_m = \Omega/g \rightarrow \infty$ as the entire medium is then effectively modulated at the same time [Fig. 9(f)]. Interestingly, a peculiar regime of modulation velocities:

$$\frac{c_0}{\sqrt{1 + \max(\delta\varepsilon)}\sqrt{1 + \max(\delta\mu)}} < v_m$$
$$< \frac{c_0}{\sqrt{1 - |\min(\delta\varepsilon)|}\sqrt{1 - |\min(\delta\mu)|}}, \tag{19}$$

exists, where the Fourier expansion in Eq. (18) does not converge, as first pointed out by Cassedy in Ref. 135. We discuss this exotic luminal regime[120] in detail in Sec. 4.3. In the next section, we discuss the role of space–time modulation for the
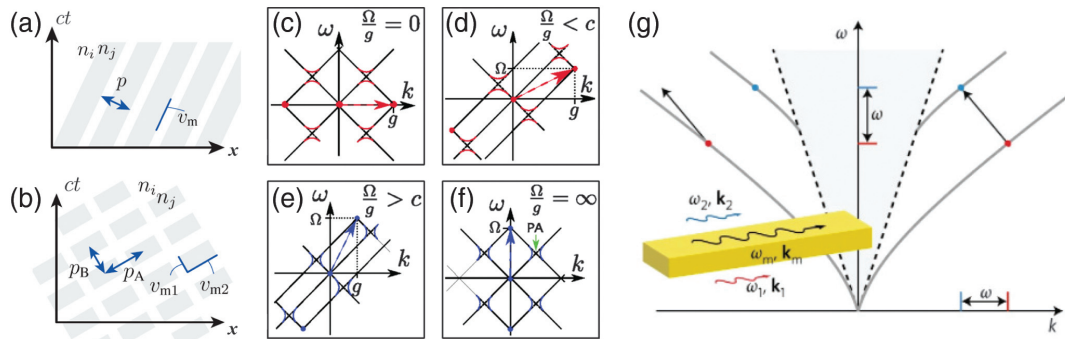
Fig. 9 (a) Space–time diagram of a space–time crystal with alternating refractive indices n_i and n_j, spatiotemporal lattice vector p and velocity v_m. (b) Double-period space–time crystal, characterized by two different lattice vectors p_A and p_B, and two different velocities v_{m1} and v_{m2}.[119] (c) The band structure for a spatial crystal with $\varepsilon \sim \cos(gz - \Omega t)$ becomes asymmetric as (d) a finite temporal component Ω, and therefore a finite modulation velocity $v_m = \Omega/g$, are introduced. This is caused by reciprocal lattice vectors (dashed arrows) acquiring a non-zero frequency component. The angle formed by the reciprocal lattice vectors with the slope of the bands determines [(c), (d)] a subluminal and [(e), (f)] a superluminal regime.[120] (g) Nonreciprocal mode-coupling in a space–time-modulated waveguide: the modulation can couple forward modes between them as their frequencies and momenta are matched by the space-time modulation, while two backward waves are not coupled, so that an impinging backward wave is effectively unchanged.[121] Figures adapted from Refs. 119, 120, and 121.

engineering of nonreciprocal scatterers, which first motivated the interest in this field.

4.1 Compact Nonreciprocal Devices without Magnetic Bias

The rise of space–time media was largely fuelled by the quest for magnet-free nonreciprocity that has earned a spotlight in the metamaterials scene of the past decade. Nonreciprocity is the violation of the Lorentz reciprocity theorem, by which swapping source and receiver leaves the scattering properties of a medium unaltered.[121] Nonreciprocal components such as isolators and circulators are crucial for duplex communications, enabling simultaneous transmission and reception at the same frequency on the same channel without parasitic reflections, as well as other applications such as laser protection from backscattering and field enhancement. The common approach to breaking this symmetry of space is the use of gyromagnetic media, where the presence of a magnetic field breaks time-reversal symmetry. One common nonreciprocal effect encountered in basic electromagnetism is Faraday rotation, whereby the rotation of the polarization of a wave passing through a gyromagnetic medium depends on the direction from which the waves are impinging on the medium. One key drawback of gyromagnetic media, however, is their requirement of strong magnetic fields and large footprint for such effects to be appreciable, leading to bulky components, incompatible with CMOS technology. Time-modulation offers the opportunity of explicitly breaking time-reversal symmetry, thereby violating reciprocity without the use of strong magnetic fields.[121]

The basic idea of using ST modulation for optical isolation may be summarized in Fig. 9(g); the modulation produces transitions between two optical states that differ in both momentum k and frequency ω, as a result, if the system hosting the waves (e.g., a waveguide) supports multiple bands, to a pair of forward propagating modes coupled by the ST modulation may not correspond a pair of backward propagating ones. Therefore, while a forward incoming wave at frequency ω_1 may be completely converted into a new mode with frequency ω_2, a backward wave at ω_1 will not be converted as it will be mismatched in frequency and/or momentum. Hence, by introducing a narrowband filter at ω_2, the system allows propagation only in the backward direction, thus achieving optical isolation,[121,132] in a similar fashion to the way a diode conducts electricity unidirectionally.[136] An equivalent way of viewing this scattering asymmetry in an extended medium is the opening of an asymmetric bandgap in the photonic dispersion of a material, allowing propagation along one direction only.[137]

Ring-resonators constitute perhaps the most promising components for electromagnetic nonreciprocity. The idea of using ring resonators for nonreciprocity makes use of the concept of angular momentum biasing [Fig. 10(a)]; a circular, directional bias splits the degeneracy between clockwise and anticlockwise states, effectively mimicking the Zeeman splitting of atomic physics [Fig. 10(b)]. In practice, this can be achieved with, e.g., three elements periodically modulated with a 120-deg phase difference between them [Fig. 10(c)]. Let us consider the two-port system formed by two linear waveguides coupled to the biased ring resonator shown in Fig. 10(d). Due to the splitting between clockwise and anticlockwise states, if the channel waveguide (on the right of the ring in the panel) is excited at a frequency resonant with the anticlockwise mode from the bottom port, its power will be mainly rerouted by the ring resonator into the drop channel (left of the ring). On the contrary, a wave impinging from the top of the waveguide, which would normally couple to the clockwise state, would now be off-resonance, thus coupling poorly to the mode of the resonator and being largely transmitted to the bottom port of the channel waveguide.[138] This strategy can be used to realize electromagnetic circulators, as shown in Figs. 10(f)–10(h). A circulator consists of three ports, and its purpose is to enable transmission from port 1 to port 2, port 2 to port 3, and port 3 to port 1, while
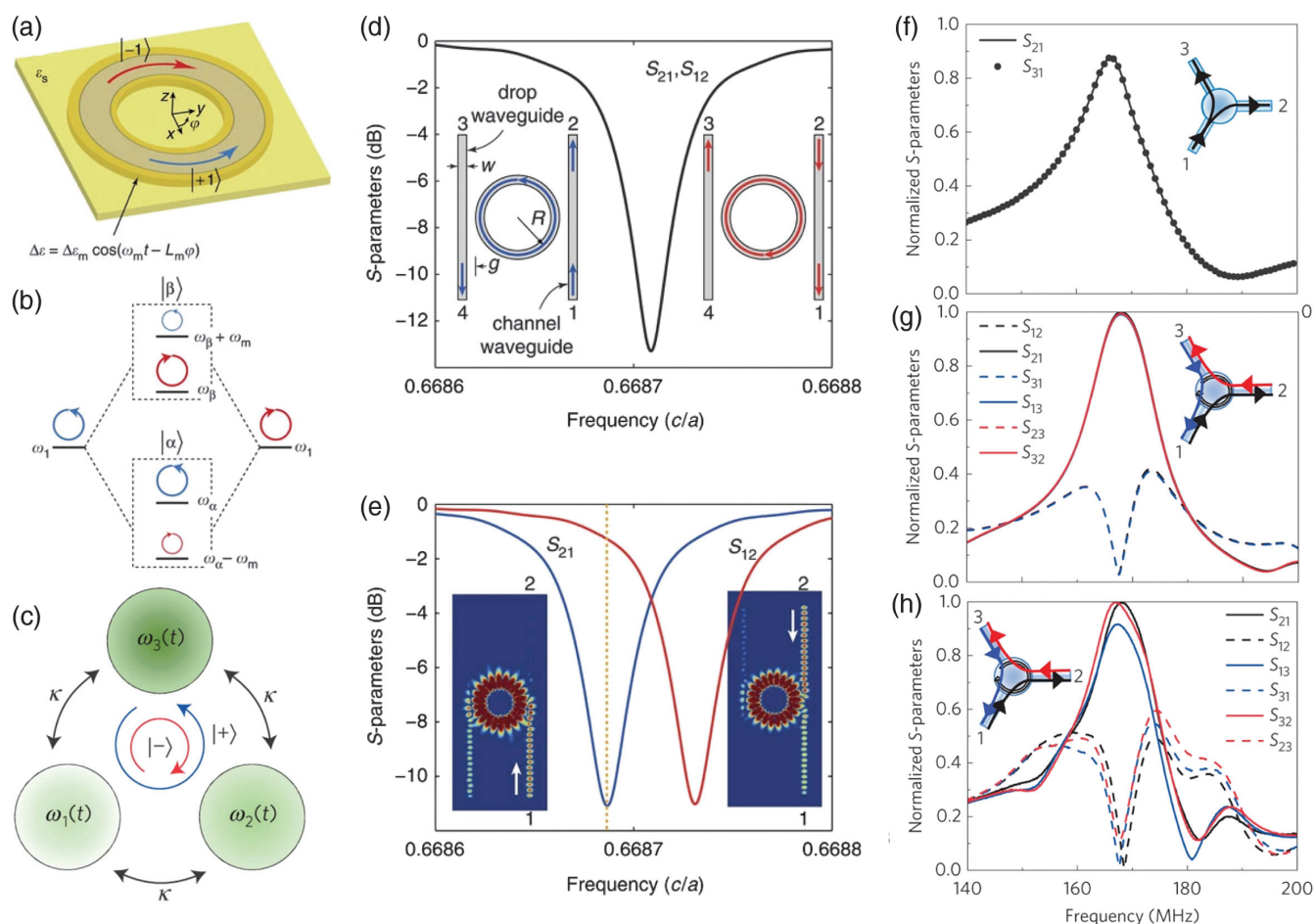
Fig. 10 (a)–(c) Angular momentum biasing: a directional modulation along a ring resonator splits the degeneracy between clockwise and anticlockwise traveling states (a),[138] in analogy with the Zeeman splitting of electronic states in a magnetic field (b),[138] this can be realized by discretizing the elements of the ring, e.g., periodically modulating three strongly coupled resonators, with a phase of 120 deg between them (c).[139] (d) Example of operation of a nonreciprocal ring resonator coupled to two waveguides: excitation from the bottom (top) of the channel waveguide (on the right of the ring) excites a counterclockwise (clockwise) mode, whose resonant frequency has been offset from the one of the clockwise (counterclockwise) mode, so (e) the direction of excitation determines the efficiency of the coupling to the resonator, and hence of the transmission to the output port of the channel waveguide.[138] (f), (g) Theoretical and (h) experimental performance of an RF circulator made with angular-momentum biased resonators: (f) and (g) the reciprocal response in the absence (f) and presence (g) of angular biasing, and (h) the performance of the experimental implementation of the circulator.[139] Figures adapted from Refs. 138 and 139.

impeding transmission in the opposite sense (i.e., $2 \rightarrow 1$, $3 \rightarrow 2$, and $1 \rightarrow 3$). Figure 10(f) shows the transmission from channels 1 to 2 and 1 to 3 in the absence of angular-momentum bias, which is perfectly symmetric. Once the bias is turned on, backward propagation is forbidden, as shown in simulations [Fig. 10(g)] and experimental data [Fig. 10(h)].[139] Other electromagnetic implementations have been realized with silicon waveguides,[133] as well as microstrip transmission lines,[130] with modulation frequencies ranging from hundreds of MHz to tens of GHz.

Multiple extensive reviews on space–time modulation focusing on nonreciprocity have recently been published, so we refer the reader to them for further details and move on to illustrate further opportunities for space–time media.[121,140]

4.2 Synthetic Motion with Space–time Media

The interaction of waves with moving bodies is at the origin of a myriad of physical phenomena, such as the Doppler effect, the Fresnel drag by which a moving medium drags light, or even the generation of hydroelectricity.[18,141–143] Moreover, the electromagnetic response of a moving system is inherently nonreciprocal, as it is associated with a broken time-reversal symmetry.[144–146] In fact, flipping the arrow of time also requires flipping the velocity of all the moving components, leading thereby to a distinct optical platform. The nonreciprocity and the non-Hermitian nature of the electromagnetic response of moving matter can enable unidirectional light flows,[146] classical and quantum non-contact friction,[147–150] and parametric amplification[146,151–153] among others.[3]

Unfortunately, it is impractical to take technological advantage of many of the features highlighted in the previous paragraph, because a realistic value for the velocity of a moving body is many orders of magnitude smaller than the speed of light. Interestingly, the actual physical motion of a macroscopic body may be imitated by a drift current in a solid state material with high mobility.[149,150,154–158] For example, it was recently experimentally verified that drifting electrons in graphene can lead to nonreciprocity at terahertz frequencies and to a Fresnel drag.[159,160] A different way to realize an effective moving response without any actual physical motion is through a traveling wave space–time modulation.[119,124,126,135,161,162] Such a solution is discussed next in detail.

A system featuring a traveling-wave-type modulation is characterized, in the dispersionless limit, by the following constitutive relations:

$$\begin{pmatrix} \mathbf{D} \\ \mathbf{B} \end{pmatrix} = \begin{pmatrix} \varepsilon(x - v_m t, y, z)\mathbf{1} & 0 \\ 0 & \mu(x - v_m t, y, z)\mathbf{1} \end{pmatrix} \cdot \begin{pmatrix} \mathbf{E} \\ \mathbf{H} \end{pmatrix}, \tag{20}$$

where v_m is the modulation speed [Fig. 11(a)]. This form of modulation in space and time imparts a synthetic motion to the material response along the x direction with a uniform speed v_m. This property implies that with a suitable coordinate transformation one can switch to a frame where the material response is time-invariant. In fact, a Galilean transformation of coordinates

$$x' = x - v_m t, \quad y' = y, \quad z' = z, \quad t' = t, \tag{21}$$

preserves the usual structure of Maxwell's equations, with the transformed fields related to the original fields as follows $\mathbf{D}' = \mathbf{D}$, $\mathbf{B}' = \mathbf{B}$, $\mathbf{E}' = \mathbf{E} + \mathbf{v_m} \times \mathbf{B}$, $\mathbf{H}' = \mathbf{H} - \mathbf{v_m} \times \mathbf{D}$, and $\mathbf{v_m} = v_m \hat{\mathbf{x}}$. In the new coordinates, the constitutive relations are time-independent

$$\begin{pmatrix} \mathbf{D}' \\ \mathbf{B}' \end{pmatrix} = \begin{pmatrix} \hat{\varepsilon}'(\mathbf{r}') & \hat{\xi}'(\mathbf{r}') \\ \hat{\zeta}'(\mathbf{r}') & \hat{\mu}'(\mathbf{r}') \end{pmatrix} \cdot \begin{pmatrix} \mathbf{E}' \\ \mathbf{H}' \end{pmatrix}, \tag{22}$$

with $\mathbf{r}' = \mathbf{r} - \mathbf{v_m} t$ and the transformed effective parameters given as

$$\hat{\varepsilon}' = \varepsilon \left(\frac{1}{1 - \varepsilon\mu v_m^2} \mathbf{1}_t + \hat{\mathbf{x}} \otimes \hat{\mathbf{x}} \right), \tag{23}$$

$$\hat{\mu}' = \mu \left(\frac{1}{1 - \varepsilon\mu v_m^2} \mathbf{1}_t + \hat{\mathbf{x}} \otimes \hat{\mathbf{x}} \right), \tag{24}$$
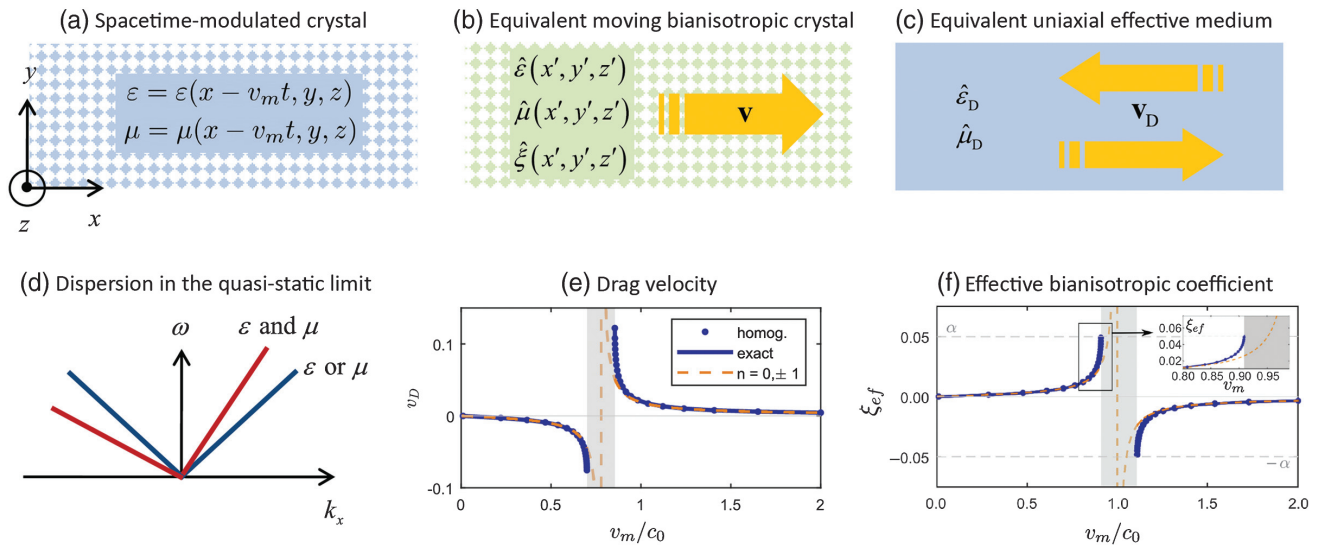

Fig. 11 (a)–(c) A synthetic space–time-modulated crystal (a) is formally equivalent to a fictitious moving bianisotropic time-invariant crystal (b) when $v_m < c_0$. The velocity of the equivalent moving crystal is identical to the modulation speed $\mathbf{v_m}$; in the long-wavelength limit, the system response can be homogenized (c) and the crystal behaves as a uniaxial dielectric moving with speed $\mathbf{v_D}$. The sign of v_D is not necessarily coincident with the sign of v. (d) Dispersion of waves in the effective medium as shown in (c). When only one of the material parameters is spatiotemporally modulated, the dispersion is symmetric, and the equivalent drag velocity vanishes (blue lines). However, when both ε and μ are modulated, the dispersion is asymmetric (red lines, assuming $v_D > 0$). The waves that propagate in the direction of $\mathbf{v_D}$ have a larger group velocity than the waves that propagate in the opposite direction.[161] (e) Drag velocity v_D and (f) effective bianisotropic coefficient ξ_{ef} as a function of the modulation speed v_m for a representative space–time-modulated crystal: the velocity of the equivalent moving medium and the magnetoelectric coupling coefficient flip sign in the transition from the subluminal to the superluminal regime. The luminal regime is marked as a shaded area in (e) and (f). Figures adapted from Ref. 163.

$$\hat{\xi}' = -\hat{\zeta}' = \frac{-\varepsilon\mu}{1 - \varepsilon\mu v_m^2} \mathbf{v_m} \times \mathbf{1}. \tag{25}$$

In the above, $\mathbf{1}_t = \hat{\mathbf{y}} \otimes \hat{\mathbf{y}} + \hat{\mathbf{z}} \otimes \hat{\mathbf{z}}$ and $\otimes$ represents the tensor product of two vectors. As seen, the coordinate transformation originates a bianisotropic-type coupling determined by the magnetoelectric tensors $\hat{\xi}'$ and $\hat{\zeta}'$,[164] such that the electric displacement vector $\mathbf{D}'$ and the magnetic induction $\mathbf{B}'$ depend on both the electric and magnetic fields $\mathbf{E}'$ and $\mathbf{H}'$. Indeed, as further discussed below, one of the peculiar features of the traveling-wave space–time modulation is that it mixes the electric and magnetic responses, leading to the possibility of a giant bianisotropy in the quasistatic limit.[161,163]

The new coordinate system is not associated with an inertial frame. An immediate consequence of this property is that the vacuum response does not stay invariant under the coordinate transformation [Eq. (21)]. Usually, this does not create any difficulties, but it is relevant to mention that it is also possible to obtain a time-invariant response with a Lorentz coordinate transformation. Such a solution is restricted to subluminal modulation velocities, and thereby the Galilean transformation is typically the preferred one.

Interestingly, the constitutive relations [Eq. (22)] in the new coordinate system are reminiscent of those of a moving dielectric medium.[144] Due to this feature, the electrodynamics of space–time media with traveling wave modulations bears many similarities to the electrodynamics of moving bodies.[161] Yet, it is important to underline that a space–time-modulated dielectric crystal is not equivalent to a moving dielectric crystal. In other words, impressing a time modulation on the parameters of a dielectric photonic crystal is not equivalent to setting the same photonic crystal into motion. A moving dielectric crystal would have a bianisotropic response in a frame where its speed v_m is nontrivial, very different from the constitutive relations [Eq. (20)]. Below, we revisit this discussion in the context of effective medium theory.

Even though the space–time-modulated dielectric system is not equivalent to a moving dielectric, its response can be precisely linked to that of a fictitious moving medium in the subluminal case. In fact, as previously noted, a suitable Lorentz transformation makes the response [Eq. (20)] of a space–time system independent of time, analogous to Eq. (22). Thus, the original constitutive relations Eq. (20) are indistinguishable from those of a hypothetical moving system with a bianisotropic response in the co-moving frame of the type [Eq. (22)]. In other words, the synthetic motion provided by the traveling wave modulation imitates the actual physical motion of a fictitious time-invariant bianisotropic crystal [Fig. 11(b)].

The previous discussion is completely general, apart from the assumption of a traveling wave modulation. In the following, we focus our attention on periodic systems and in the long wavelength regime. Effective medium methods have long been used to provide a simplified description of the wave propagation in complex media and metamaterials.[165–168] The effective medium formalism is useful not only because it enables analytical modeling of the relevant phenomena but also because it clearly pinpoints the key features that originate the peculiar physics of a system.

The standard homogenization approach is largely rooted in the idea of "spatial averaging," so the effective response describes the dynamics of the envelopes of the electromagnetic fields.[18] In particular, in the traditional framework, there is no

time averaging. Due to this reason, standard homogenization approaches are not directly applicable to spacetime crystals, where the microscopic response of the system depends simultaneously on space and on time. At present, there is no general effective medium theory for spacetime crystals. Fortunately, the particular class of spacetime crystals with traveling wave modulations can be homogenized using standard ideas.[163,169,170] In fact, since a traveling wave modulated spacetime crystal is virtually equivalent to a moving system, it is possible to find the effective response with well-established methods by working in the co-moving frame (primed coordinates) where the medium response is time-invariant.[163]

To illustrate these ideas, we consider a 1D photonic crystal such that the permittivity ε and permeability μ are independent of the y and z coordinates. It is well known that, for stratified systems, the components of the $\mathbf{E}$ and $\mathbf{H}$ fields parallel to the interfaces (y and z components) and the components of the $\mathbf{D}$ and $\mathbf{B}$ fields normal to the interfaces (x components) are constant in the long-wavelength limit,[171] i.e., when the primed field envelopes vary sufficiently slowly in space and in time. Taking this result into account, one can relate the spatially averaged $\langle\mathbf{D}'\rangle$ and $\langle\mathbf{B}'\rangle$ to the spatially averaged $\langle\mathbf{E}'\rangle$ and $\langle\mathbf{H}'\rangle$.[163] The effective parameters in the original (laboratory) frame can then be found with an inverse Galilean (or Lorentz) transformation. Such a procedure leads to the following constitutive relations in the lab frame:

$$\begin{pmatrix} \langle\mathbf{D}\rangle \\ \langle\mathbf{B}\rangle \end{pmatrix} = \begin{pmatrix} \hat{\varepsilon}_{\mathrm{ef}} & \xi_{\mathrm{ef}}\hat{\mathbf{x}} \times \mathbf{1} \\ -\xi_{\mathrm{ef}}\hat{\mathbf{x}} \times \mathbf{1} & \hat{\mu}_{\mathrm{ef}} \end{pmatrix} \cdot \begin{pmatrix} \langle\mathbf{E}\rangle \\ \langle\mathbf{H}\rangle \end{pmatrix}, \tag{26}$$

where $\hat{\varepsilon}_{\mathrm{ef}}$, $\hat{\mu}_{\mathrm{ef}}$, and ξ_{ef} are some parameters that can be written explicitly in terms of the permittivity and permeability profiles $\varepsilon(x)$ and $\mu(x)$.[163] It turns out that when only one of the material parameters is modulated in spacetime the magnetoelectric coupling coefficient ξ_{ef} vanishes and the effective medium behaves as a standard uniaxial dielectric.[161,163] For example, if the material permeability is independent of space and time, then $\xi_{\mathrm{ef}} = 0$ and $\hat{\mu}_{\mathrm{ef}} = \mu\mathbf{1}$, for any permittivity profile $\varepsilon(x)$. This property can be intuitively understood by noting that when μ is a constant, the "microscopic" constitutive relation $\mathbf{B} = \mu\mathbf{H}$ implies that the averaged fields are also linked by $\langle\mathbf{B}\rangle = \mu\langle\mathbf{H}\rangle$, which corresponds to a trivial effective magnetic response. Note that this argument is only justified in the static limit, as in the dynamical case the second-order spatial dispersion effects may lead to artificial magnetism.[166,172]

Remarkably, when both ε and μ are modulated in spacetime, ξ_{ef} can be nontrivial. In other words, notwithstanding that at the microscopic level there is no magnetoelectric coupling [Eq. (20)], the effective medium is characterized by a bianisotropic response in the static limit. While it is not unusual that the complex wave interactions in a metamaterial without inversion symmetry can result in a magnetoelectric coupling,[164] having a nontrivial bianisotropic response in the long wavelength limit is a rather unique result. (For completeness, we point out that some antiferromagnets, such as chromium oxide, may be characterized by an intrinsic axion-type bianisotropic response in the static limit.)[173,174] In fact, in typical time-invariant systems, the electric and magnetic fields are decoupled in the static limit. Thereby, the electric and magnetic responses of any conventional metamaterial are necessarily decoupled in the static limit and there is no bianisotropy. In contrast, for a space–time-modulated system, the electric and magnetic fields are never fully

decoupled, as the time modulation of the material implies always some nontrivial time dynamics. The strength and sign of ξ_{ef} can be tuned by changing the modulation speed and the profiles of the permittivity and permeability. As shown in Fig. 11(f), ξ_{ef} can be exceptionally large for modulation speeds approaching the speed of light in the relevant materials. This results in giant nonreciprocity, as has also been shown through Floquet–Bloch expansions.[175] The transition from the subluminal to the superluminal regime is marked by a change in sign of ξ_{ef}. Furthermore, it can be shown that constitutive relations [Eq. (26)] are identical to those of a fictitious moving anisotropic dielectric characterized in the respective co-moving frame by the permittivity $\hat{\varepsilon}_D$ and by the permeability $\hat{\mu}_D$. The equivalent medium moves with a speed v_D with respect to the lab frame. The parameters $\hat{\varepsilon}_D$, $\hat{\mu}_D$, and v_D are determined univocally by $\hat{\varepsilon}_{ef}$, $\hat{\mu}_{ef}$, and ξ_{ef}.[163] In general, v_D may be rather different from the modulation speed v_m, both in amplitude and sign. The velocity v_D can be nonzero only if ε and μ are both modulated in spacetime, i.e., only if $\xi_{ef} \neq 0$. Therefore, it follows that a space–time-modulated photonic crystal can imitate precisely the response of a moving dielectric in the long wavelength limit. Remarkably, the velocity of the equivalent moving medium can be a very significant fraction of c_0 [Fig. 11(e)]. Thus, space–time-modulated systems are ideal platforms to mimic on a table-top experiment the electrodynamics of bodies moving at relativistic velocities, the only caveat being that some degree of frequency mixing will, in general, occur upon propagation in a space–time medium.

In particular, similar to a moving medium, a space–time-modulated crystal can produce a drag effect.[161] Specifically, a wave copropagating with the equivalent moving medium, i.e. toward the direction $\text{sgn}(v_D)\hat{x}$, moves faster than a wave propagating in the opposite direction, due to the synthetic Fresnel-drag effect.[143] A clear fingerprint of the Fresnel drag can be detected in the dispersion of ω versus k of the electromagnetic modes of the spacetime crystal. In fact, when both ε and μ are modulated in time, the slopes of the dispersion of the photonic states near $k = 0$ depend on the direction of propagation of the wave. The dispersion of the waves that copropagate with the equivalent moving medium exhibits a larger slope than the dispersion of the modes that propagate in the opposite direction, as shown in Fig. 11(d). Interestingly, these slopes are predicted exactly by the discussed effective medium theory, and thereby the homogenization theory is expected to be rather accurate and useful to characterize excitations that vary sufficiently slowly in space and in time. Furthermore, the effective medium theory is exact for all frequencies when the parameters of the crystal are matched: $\varepsilon/\mu = \text{const.}$. In fact, the dispersion of a matched photonic crystal is generally linear for all frequencies. However, as we show in the next section, even this statement can be violated in an exotic class of spacetime media recently termed luminal metamaterials.

4.3 Luminal Amplification and Spatiotemporal Localization

If the speed of a space–time modulation falls within the modulation velocity regime in Eq. (19) (the extent of this luminal regime increases with the modulation amplitude), the relevant wave physics changes dramatically, entering a very peculiar unstable phase whose underlying mechanism is, however, completely distinct from the parametric amplification processes

described in Secs. 2 and 3.[120] In this regime, all forward bands become almost degenerate, as the frequency-momentum reciprocal lattice vectors effectively align with the forward bands. This regime marks a transition between the subluminal and superluminal regimes in Figs. 9(d) and 9(e), respectively. Due to the resulting strong degeneracy between forward-traveling waves, the eigenmodes of these luminal systems cannot be written in the Bloch form:[176] the effect of the modulation, in fact, is to couple all of the forward bands, such that an impinging wave would emerge as a supercontinuum, or frequency comb. Such a transmission process is shown in Figs. 12(a)–12(d); the waves are compressed into a train of pulses, and both the total energy of the system and its compression increase exponentially with respect to the propagation length (or time) in the luminal medium, as well as the amplitude and rate of the modulation.

In real space, this amplification process can be viewed as the trapping of field lines by the synthetically moving grating.[178] The wave dynamics in a luminal medium can be captured by the approximate equation for the energy density U:

$$\frac{\partial \ln U}{\partial t'} = \frac{v_m + c_l}{2}\left(\frac{\partial \ln \mu}{\partial X} + \frac{\partial \ln \varepsilon}{\partial X}\right) + (v_m - c_l)\frac{\partial \ln U}{\partial X},$$
(27)

where v_m is the grating velocity, $c_l(X) = (\varepsilon\mu)^{-1/2}$ and $X = x - v_m t$ and $t' = t$ are moving coordinates, which can be solved by successive iterations.[177] Note that this equation becomes exact if $\varepsilon = \mu$ everywhere (impedance-matching). The characteristic feature of the luminal regime is the presence of points along the grating where the local phase velocity $c_l(X)$ of the waves matches the velocity v_m of the grating [crossings between the black, dashed horizontal line, and the green sinusoidal grating profile in Fig. 12(b)]. The presence of these velocity-matching points implies that the lines of force are trapped within each period of the grating, merely subject to the first term in Eq. (27), which acts as an energy source term, resulting from the spatiotemporal change in ε and μ. In fact, these local gradients in the electromagnetic parameters will pump energy into the waves, or deplete them, based on their sign, whereas the phase velocity of the waves in the region adjacent to the velocity-matching points determines whether these will function as attractors [$\pi/2$ in Fig. 12(b)] or repellors [$3\pi/2$ in Fig. 12(b)] as a result of the Poynting flux driving power toward them or away from them.[179] It has been noted that this completely linear mechanism results in pulse compression or expansion.[180] On the other hand, as the modulation velocity approaches the edges of the luminal regime, a localization transition takes place, before which the response of the system is characterized by strong oscillations in time consisting of periodic field compression and expansion,[176] as shown in Figs. 12(e)–12(g). Importantly, luminal amplification does not rely on backscattering, as opposed to parametric amplification, and in fact it occurs just as well in a system that is impedance-matched everywhere in spacetime, in sharp contrast to parametric amplification, which relies on time-reversal as explained in Sec. 3.

4.4 Space–Time Metasurfaces

Most implementations of time-varying and space–time-varying systems are hard to achieve in bulk, as any modulation mechanism, e.g., a pump pulse, would generally need to impinge on
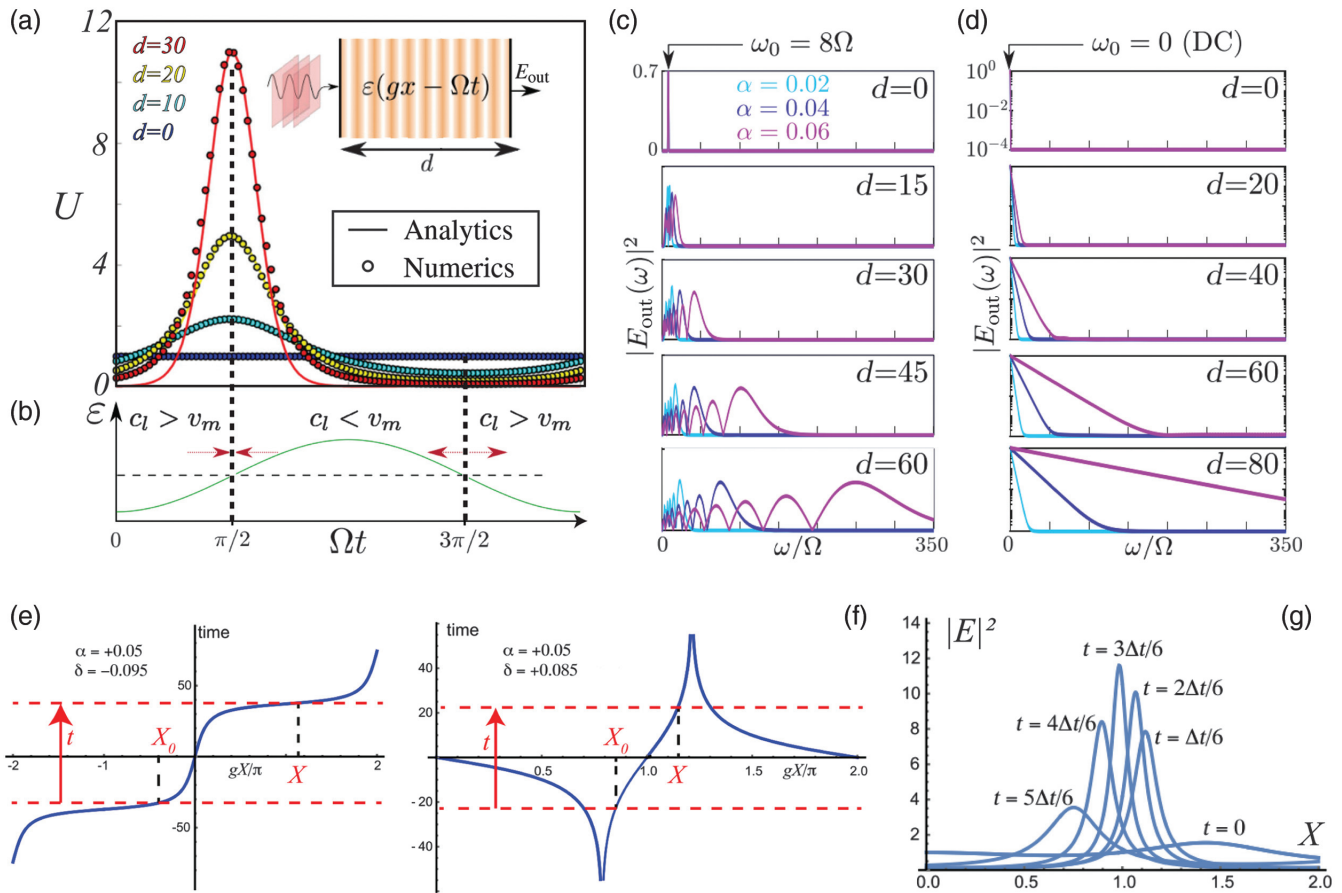
Fig. 12 (a) Time dependence of the electric field intensity at the output port transmitted through different thicknesses (blue to red) d of luminal crystal. (b) In the gain region, the permittivity gradient is positive, and vice versa. The gain is maximum at the points (in time or space) where the velocity of the waves matches the velocity of the grating. (c), (d) Power spectra of the transmitted waves (c) for input frequency $\omega_0 = 8\Omega$, with Ω the modulation frequency, and (d) for a DC input field ($\omega_0 = 0$), showing the frequency generation responsible for the overall gain.[120,177] (e), (f) Trajectories of a point of constant phase along the spacetime variable $X = x - v_m t$: (e) outside of the localization regime (resulting in oscillations that periodically compress and decompress the pulse) and (f) within the localization regime, resulting in the amplification and compression described in (a)–(d).[176] Figures adapted from Refs. 120, 176, and 177.

the system from an additional direction. In addition, field penetration into a bulky structure is generally inhomogeneous, so in practice only a small surface layer of a bulk medium would effectively be modulated. These considerations, combined with the ease of fabrication of metasurfaces compared to bulk metamaterials, have led to a concentration of research interest in space–time metasurfaces, whereby a traveling-wave modulation is applied to the surface impedance of a thin sheet, with proposals covering a wide range of ideas and applications, some of which are shown in Fig. 10.

Systems such as isolators [Fig. 13(a)], nonreciprocal phase shifters [Fig. 13(b)], and circulators [Fig. 13(c)] using space–time-modulated metasurfaces were designed, extending magnet-free nonreciprocity to surface implementations.[104,111,182,183] A promising idea to exploit these concepts in practice, at least at low frequencies, has come in the form of space–time-coding digital metasurfaces [Fig. 13(d)]; these systems consist of arrays of elements whose impedances are designed to take a discrete set of values, so the overall response of the structure can be

encoded as an array of bits (if only two values exist for each element).[184] Switching the individual impedances of a voltage-controlled array of such elements can enable exquisite control over the metasurface response in a system whose design can be systematically described using information theory concepts to tailor shape and direction of electromagnetic beams [Fig. 13(e)],[114] as well as to perform photonic analog computing.[185] Furthermore, close to the luminal regime, opportunities for nonreciprocal hyperbolic propagation,[162] as well as vacuum Čerenkov radiation[186] using space–time metasurfaces have recently been highlighted.

Another application of space–time metasurfaces that was recently proposed is that of power combining of waves, a long-standing challenge in laser technology. Here, the strategy consists of using a spatiotemporal modulation of a surface to effectively trade the difference in angle of incidence between a discrete set of incoming waves with identical frequency in exchange for a difference between the (equally spaced) frequencies of the outgoing waves, which emerge at
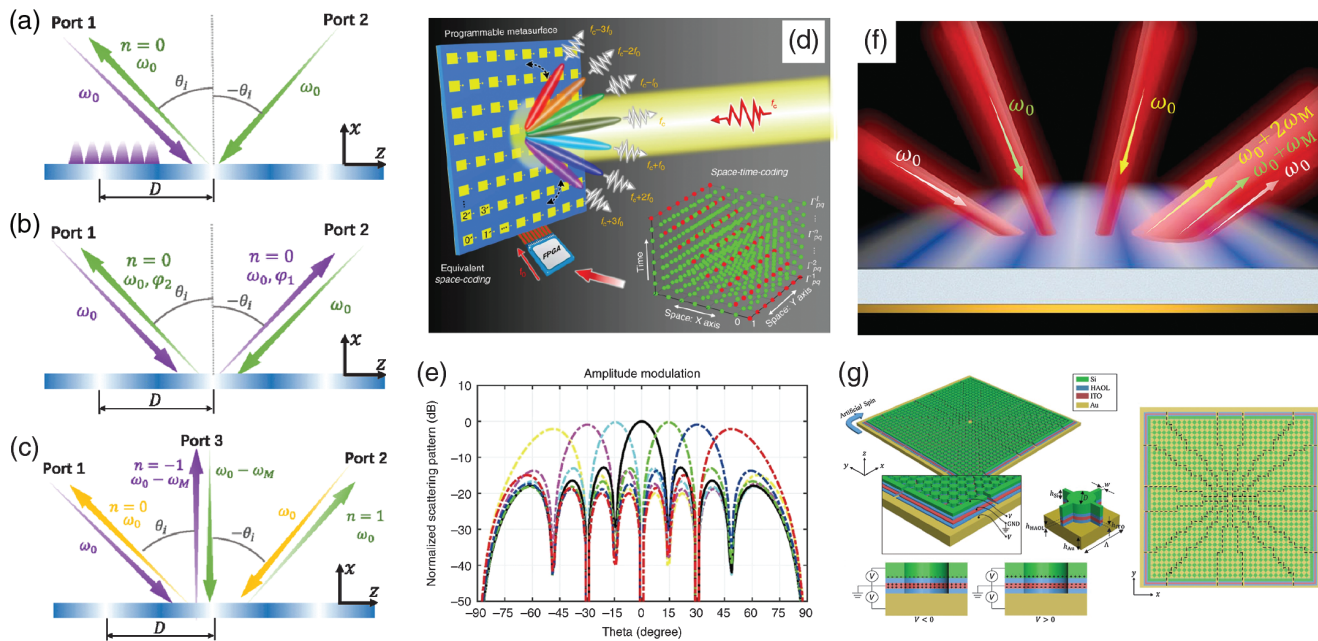
Fig. 13 Examples of applications of space–time metasurfaces. (a) An isolator based on the unidirectional excitation of evanescent modes. (b) Waves scattering off an STM experience a nonreciprocal phase shift. (c) An STM-based circulator.[104] (d) Illustration of an experimentally realized space–time coding metasurface, consisting of a square array of individual voltage-controlled elements with binary impedance values, enabling encoding and imprinting of arbitrary phase and amplitude modulation onto different scattered harmonics for (e) beam-steering and shaping.[114] (f) Illustration of wave power combining using STMs: incoming waves with frequency ω_0 coming from a discrete range of different angles can be scattered toward the same outgoing direction by imprinting the necessary frequency-wavevector shifts via the STM.[108] (g) A proposal of an angular momentum-biased metasurface for the generation of orbital angular momentum states: each azimuthal section is temporally modulated with a different relative phase, imparting the necessary angular-momentum bias. Figures adapted from Refs. 104, 108, 114, and 181.

the same angle, as shown in Fig. 13(f).[108] More exotic ideas include angular-momentum-biased metasurfaces [Fig. 13(g)], which can impart a geometric phase on the impinging waves, and engineer photonic states with finite orbital angular momentum and optical vortices.[110,181] Finally, the concept of space–time metasurfaces has recently been imported into the quantum realm, promising full control of spatial, temporal, and spin degrees of freedom for nonclassical light, with several opportunities for the generation of entangled photonic states, thereby anticipating a whole new scenery for this field to expand toward.[187]

4.5 Further Directions

Among new directions for space–time media, dispersive effects offer additional knobs for mode-engineering,[188] for which much still remains to be explored. Interestingly, spatial dispersion may be effectively engineered into a material via time-modulation, just as temporal dispersion arises from spatial structure.[189] Chiral versions of synthetically moving and amplifying electromagnetic media, mimicking the Archimedean screw for fluids, have recently been proposed, and may be realized with circularly polarized pump-probe experiments.[190] Topology also occupies a prime seat, with Floquet topological insulators having been realized in acoustics,[191] and theoretically proposed for

light.[192] Further related opportunities have been demonstrated for photonic realizations of the Aharonov–Bohm effect,[193] as well as for the engineering of Weyl points (three-dimensional spectral degeneracies analogous to Dirac points, signatures of topological states) within spatially 2D systems, exploiting a synthetic frequency dimension.[194] The idea of space–time media has also been formalized in the interesting mathematical formulation of "field patterns." These objects arise from the consecutive spatial and temporal scattering in a material that features a checkerboard-like structure of its response parameters in space and time and may offer new angles to study space–time metamaterials in the future.[170,195,196] Finally, besides photonic systems, nonelectromagnetic dynamical metamaterials have already acquired significant momentum, with several theoretical proposals[197–199] and experimental realizations, including asymmetric charge diffusion,[200] nonreciprocity,[145,201,202] Floquet topological insulators[191] and topological pumping[203] among many others. In particular, digitally controlled acoustic meta-atoms have recently attracted significant interest to probe time-modulation physics in acoustics.[204,205]

Having discussed the wealth of potential new physics enabled by temporally and spatiotemporally modulated media, we now turn our attention to the latest technological advances toward experimental implementations in photonics, and their related challenges.

5 Experimental Advances and Challenges in All-Optical Implementations

The experimental realization of time-varying effects constitutes a new, broad, and fruitful field of research across the wider wave-physics and engineering spectrum. Implementation in optics and more particularly in nanoscale architectures and metasurfaces offers new opportunities to address both fundamental open questions in wave physics as well as material science, and potentially groundbreaking technological pathways, such as low-footprint ultrafast optical modulators and nonreciprocal components. This is particularly challenging due to the need for modulating a medium on a temporal scale similar to the optical frequency of the light field. Time-varying effects have been demonstrated in mechanical,[206] magnetic,[207] acousto-optic,[208] opto-mechanical,[209] and electronic systems.[133] In particular, electromagnetic metasurfaces can be modulated via mechanical actuation, chemical reactions, or phase-change materials, as well as electrically.[116] Nevertheless, their slow modulation speed compared to near-optical timescales makes these poor candidates for achieving sizable frequency shifts and other time-varying effects in the visible or near-infrared ranges. The following section focuses on experimental realizations of time-varying media in these optical frequency ranges. Emphasis is placed on metasurfaces as these have subwavelength thicknesses that allow for purely temporal modulations of the medium. In a metasurface, the various constraints of bulk media such as absorption losses or self-broadening are avoided, and the propagation of the modulating or probe beam in the medium does not need to be taken into account. We will review first the state of the art of time-varying photonics experiments using nonlinear optical processes in semiconductors, more specifically their most common implementations: epsilon near zero (ENZ) materials, hybrid ENZ platforms, and high-index dielectrics. We will then discuss emerging paths to implement all-optical ultrafast modulation within new structures or materials, such as quantum wells, magnetic materials, multilayered metamaterials, and 2D materials.

5.1 Photocarrier Excitation and Nonlinear Optical Modulation

Due to their wide variety of implementations and frameworks, as well as their ultrafast nature, nonlinear optical interactions have proven to be a fertile ground for the development of time-varying systems at optical frequencies. In particular, modulation effects originated by short laser pulses interacting with a nonlinear medium occur on sub-ps timescales, well beyond the reach of electro-optic modulation, and very close to the time of an optical cycle (1 to 10 fs regime). Optical modulation of a medium stems from a change in ε, the relative permittivity, due to the nonlinear response in a material. In semiconductors, these effects are often driven by out-of-equilibrium electronic populations, called hot-electrons. Nonlinear effects in semiconductors arise because of electron excitation of either real or imaginary states. Transitions through real states are realized by photocarrier excitation, that is intraband or interband transitions of the electrons within the active medium. The redistribution of electrons within the valence and/or conduction bands will affect the permittivity and thus the refractive index of the material on timescales limited either by the rate of transfer of energy from the light beam to the electrons or by the light

pulse duration. This allows for sub-ps modulation of ε in a variety of media of interest for photonics, including dielectrics and metals. Transitions through virtual states are, on the other hand, much faster but lack the strength of photocarrier excitations: nonlinear processes via virtual states, such as four-wave-mixing and sum-frequency-generation, usually exhibit low efficiencies. Both photocarrier excitation and nonlinear optical modulation induce ultrafast modulation of ε, generally limited by the pulse duration and not material-limited. In the next section, we will discuss recent progress in nonlinear optical modulation for time-varying effects in two main platforms: epsilon-near-zero media and high-index dielectrics.

5.1.1 Epsilon-near-zero materials, transparent conducting oxides, and nonlinear optics

ENZ materials exhibit various interesting properties around their ENZ frequency, where the real part of their permittivity crosses zero, whereas the imaginary part stays relatively low. ENZ media feature guided and plasmonic modes for field enhancement, slow-light effects in waveguides and phase-matching relaxation.[210] Of particular interest are transparent conducting oxides (TCOs), degenerately doped semiconductors whose band structures allow for ENZ frequencies in the near-IR with strong optical nonlinearities. Indium tin oxide (ITO) and aluminum zinc oxide (AZO) are well-known, silicon-technology compatible TCOs with very strong nonlinear optical response,[211–214] which makes them good candidates as platforms for time-varying metasurfaces. Particularly, intraband transitions in ITO lead to a strong redistribution of the effective mass of conducting electrons and thus an efficient shifting of the plasma frequency in the material's Drude dispersion as shown in Fig. 14(a). As shown by Alam et al. in 2016,[211] order of unity modulation of the refractive index can be achieved in ITO. Keeping in mind that for an instantaneous change of index, the frequency shift due to time-refraction is proportional to $\Delta n/n$, where n is the refractive index and Δn is the index change. Strong frequency shifts can be achieved in ITO due to its low refractive index near its ENZ frequency, even for small changes Δn.

Time-refraction in pump probe experiments has been shown in bulk ITO and AZO thin-films,[215,216,219–221] with frequency shifts as strong as 58 THz[216] when the probe field and the modulation overlap [see diagram in Fig. 14(b)]. Time-refraction not only applies to the reflected and transmitted probe pulse but also to its phase conjugation and negative refraction, as shown in Figs. 14(c)–14(f). In the works of Ferrera et al.,[219] Vezzoli et al.,[220] and Bruno et al.,[216] negatively refracted and phase-conjugated signals were recorded simultaneously with the time-refracted signal, with the internal efficiencies going above unity for these ultrafast, purely time-varying signals.[220] This demonstrated the potential of these TCOs for time-varying applications, yet the strength of the modulation and signal was mostly achieved due to a significant propagation within the medium and was hampered by losses in the medium (for ITO, the penetration depth of light around the ENZ frequency is about 100 nm). Time-refraction in an 80-nm-thick ITO metasurface was demonstrated in Liu et al.'s work[222] in 2021, which in turn highlighted the need for a new understanding of the role of saturation of photocarrier excitation in the modulation of permittivity as large field intensities are now confined to significantly smaller portions of space. In this work, it was shown that, as expected, a shorter pulse will lead to a stronger shift
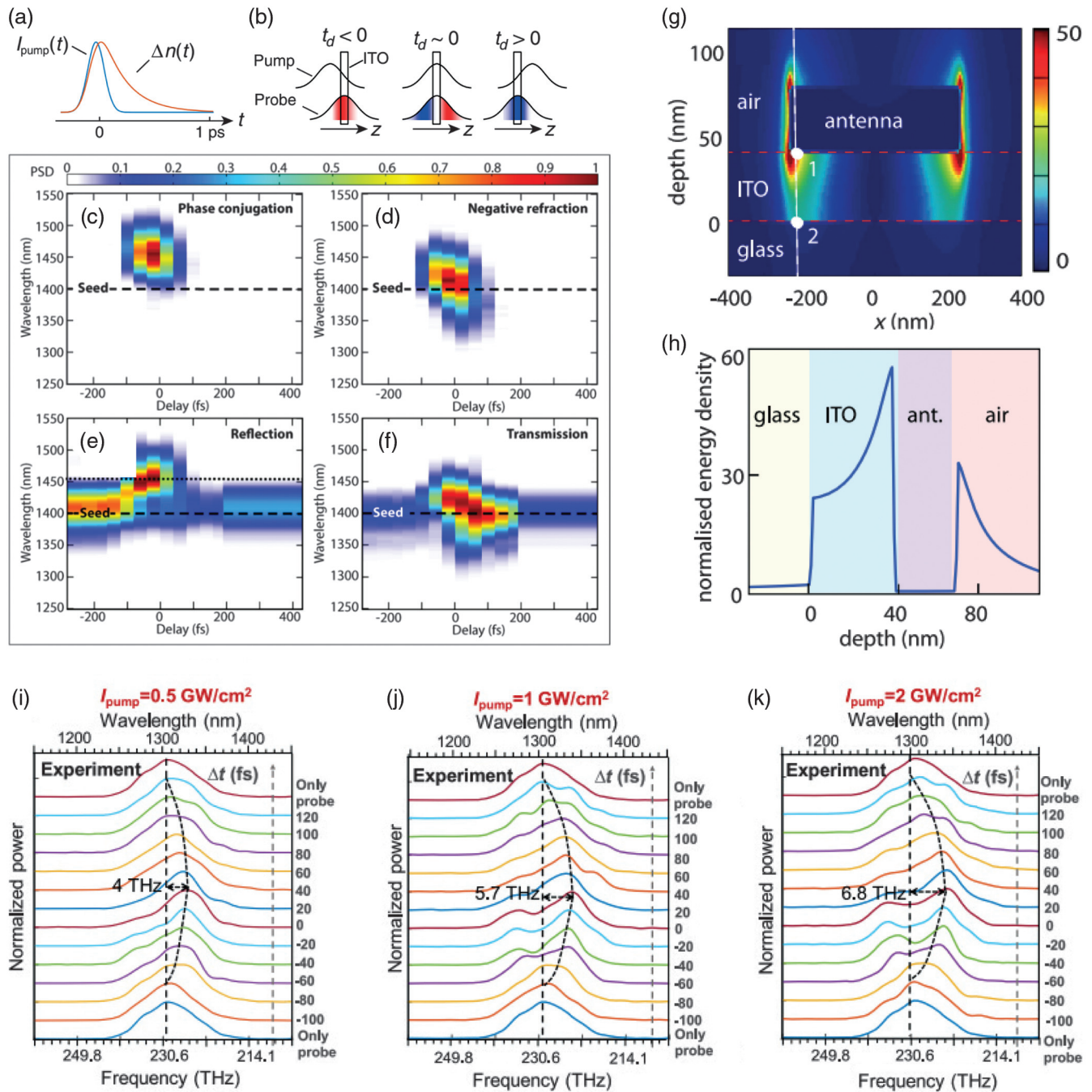
Fig. 14 (a), (b) Concept of photocarrier excitation and time-refraction in ITO:[215] (a) A pump pulse transfers energy to the electrons in the conduction band, leading to a temporal variation in the refractive index. (b) As the probe experiences different indices at different delays, its spectral content will be shifted (redshift for negative delay, blueshift for positive). (c)–(f) Measured time-refraction, phase conjugation, and negative refraction signals from a 500-nm-thick AZO slab pumped by 105 fs pulses, at an energy of 770 GW/cm² in a degenerate pump-probe experiment at 1400 nm.[216] (g) Strong coupling between a plasmonic antenna and an ENZ thin film:[217] electric field $|E|^2$ distribution obtained from FDTD for an ITO layer thickness of 40 nm and Au antenna length of 400 nm. (h) Resulting field distribution as a function of depth.[217] (i)–(k) Probe spectrum at various delays for a central wavelength of 1304 nm for 50 fs pulses in a strongly-coupled plasmonic antenna-ENZ system.[218] The increase in modulating pump intensities (0.5, 1, and 2 GW/cm²) leads to a shift near zero delay. Figures adapted from Refs. 216 to 218.

in frequency due to a larger dn/dt during the short propagation time within the ITO slab, but more interestingly, that saturation happens at lower energies for longer pulses. This indicates that predicting and measuring the ultimate material response time for short and intense modulation constitutes still an open research question.

Nanostructuring ENZ materials is a powerful strategy to increase the optical field enhancement and lead to efficient ultrafast modulation as demonstrated by Guo et al.'s work[223] with ITO nanorods. In this work, the thickness of the medium is 2.6 μm, a length sufficient to cause significant loss upon propagation. An alternative to nanostructuring the ITO to increase the field enhancement consists of exploiting the plasmonic mode exhibited by flat ENZ thin films.[224] In Bohn et al.'s work,[225] the plasmonic ENZ mode was excited using a Kretschmann configuration, leading to a change in reflectance of 45%.

While ENZ materials allow for large nonlinear responses and time-modulation, their large refractive index mismatch with air or larger-than-one-index media calls for advanced photonic architectures to ensure efficient coupling, as we will address in the next section.

5.1.2 Hybrid platforms for time-varying experiments

To compensate for the lack of interaction volume in a metasurface, good in-coupling and enhancement of the electric field is necessary to achieve strong nonlinear optical modulation. ENZ material-only metasurfaces lack strong resonant behavior, and this has prompted the community to include additional elements to achieve efficient time modulation. Well-understood and easy-to-realize, plasmonic-ENZ metasurfaces provide light coupling and local field enhancement for otherwise impedance-mismatched ENZ materials.

Plasmonic nanoantennas couple efficiently propagating radiation to their near field. When plasmonic resonances are excited, electromagnetic hot-spots form in the surrounding media. For this reason, metallic and, more particularly, Au nanoantennas have been used to couple light from the far field to a thin ENZ substrate, where the strong field enhancement leads to efficient nonlinear modulation of the medium. In addition, strong coupling of localized plasmon resonances in Au antennas with the plasmonic modes of an ENZ film can be achieved[217] [see Figs. 14(g)–14(h)]. The coupled antenna-ENZ thin film enhances the field in the ENZ medium, and strong frequency shifts originating from time-refraction, as well as efficient negative refraction, have been measured from ITO films[217,222,226] with a record 11.2 THz frequency shift being recorded at a comparatively low power of 4 GW/cm² in Pang et al.'s work[218] [Figs. 14(i)–14(k)]. Such time-varying metasurfaces are at the moment limited by the low damage threshold of the plasmonic antennas, the damage threshold of ENZ materials such as ITO or AZO being much higher. To circumvent damage threshold constraints, architectures where the optical field is localized only in the ENZ layer have been explored: Au films can be used as a perfectly conducting layer in the near-IR and IR, beneath the ENZ thin film to increase its coupling to free space. Even though this is an impedance-matching effect, it can be understood as a superposition of the suppression of reflection for p-polarized light at the Brewster angle and the suppression of transmission from the reflective layer. Such a system was used by Yang et al.,[227] a layer of In:CdO with an ENZ frequency at 2.1 μm exhibited large nonlinearities when illuminated at its Brewster angle, with the ninth harmonic being generated and measured from the

metasurface. Time-varying effects are noticeable in the harmonic spectrum, with, for example, the fifth harmonic exhibiting two peaks: a small one at $5f$ and a large, time-refracted one 48 THz below arising from the modulation of the index by the pump and the shifted frequencies being upconverted (that is a shift of about 2 THz of the probe signal due to time-refraction).

Hybrid plasmonic-ENZ systems thus present an improvement in realizing time-varying metasurfaces using the favorable properties of ENZ materials and other TCOs. This calls for further investigation of the implementation of ENZ properties in other types of metasurfaces, such as the multilayered systems presented in Sec. 5.2.3.

5.1.3 High-index dielectric metasurfaces as time-varying media

In the quest for resonantly enhanced materials for time-modulation, high-index dielectrics provide an alternative to ENZ structures, as they offer possibilities for various resonant architectures and a high damage threshold. In particular, nanoantennas with Mie resonances or bound states in the continuum allow for strong time-modulation by combining efficient coupling to the active medium and a good field enhancement. That is because even though $\Delta n/n$ is low in a high-index dielectric, the change of phase of the metasurface can be strong when the material is modulated near a resonance. Shifts in the resonance of a photonic crystal[228] were demonstrated, as well as in Mie-resonant systems, in a range of materials ranging from Si[229–231] to GaAs,[232] GaP,[233] and Ge.[234] GaAs exhibits stronger modulation efficiencies as it features a direct bandgap in the visible to near-IR region, while Si, GaP and Ge rely on indirect band gap transitions, less efficient for this class of materials.[232]

Time-refraction was observed both in Si[235] and GaAs[236] high-Q nanoantenna metasurfaces. Shcherbakov et al.[235] reported a 8.3-THz shift in the third harmonic signal from a Si metasurface with a collective Fano resonance as shown in Fig. 15(a), i.e., around 2 THz shift in the self-modulated pump signal. As shown in Fig. 15(b), this is explained by the upconversion to third harmonic of the time-refracted pump field, with the change of index of the nanoantenna cavity originating from the pump itself as well. This is a smaller shift than the best results achieved with combined plasmonic antenna-ENZ systems, but comparable to what was achieved in bulk ITO[222] and In:CdO on Au.[227] It is also worth noting that the system operates at 11 GW/cm², underlining the higher damage threshold of dielectric antennas in comparison to plasmonic antennas.

Though high-index dielectric antennas exhibit a higher damage threshold and provide more flexibility due to the tunability of the resonances by nanostructuring, as opposed to bulk ENZ properties, the interplay between the width of the resonance and that of the modulating pulse must be considered carefully. The higher the Q factor, the stronger the potential for a modulation as the field enhancement is higher at resonance, yet if the duration of the modulating optical pulse is made shorter than the resonance lifetime, to accelerate the modulation and obtain stronger time-varying effects, its spectral content will exceed the resonance bandwidth and only a modest portion will interact. This calls for nondegenerate pump-probe experiments to show the full-potential of time-varying media; Karl et al.[236] recorded the clear appearance of fringes in the probe spectrum due to time-varying effects as shown in Fig. 15(c), by independently controlling the pump pulse length via pulse chirping and the
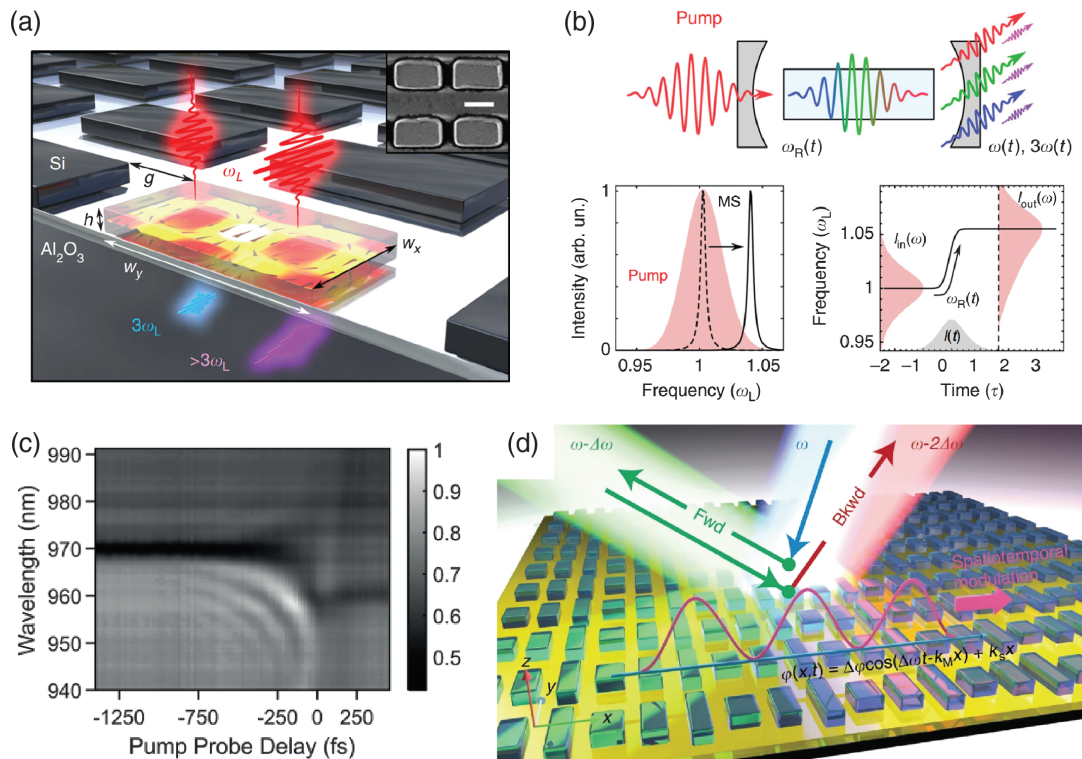
Fig. 15 (a) Schematic of a Si metasurface engineered to support collective high-Q Fano resonances.[235] (b) Schematic of the self-induced blueshift of harmonics in the resulting Si nanoantenna cavity:[235] photons in the antenna will undergo a blueshift due to the rapidly changing permittivity of the medium before being upconverted via third-harmonic generation. (c) Measured spectral evolution for an 80-fs pump pulse length in a GaAs high-Q metasurface.[236] The fringes are measured on only one side of the spectrum due to the breaking of time-reversal symmetry caused by the modulation. (d) Schematic of a nonreciprocal Si metasurface:[237] the traveling wave modulation breaks the space–time symmetry of the reflection phase change. Figures adapted from Refs. 235 to 237.

spectral content of the probe via spectral filtering of a supercontinuum pulse.

One can also take advantage of the phase shift induced by a high-index nanoantenna array; Guo et al.[237] demonstrated nonreciprocal light reflection in a Si nanobar metasurface. To this end, a spacetime modulation was induced by the interference and beating of two pump beams with a 6-nm difference in central wavelength and a nonreciprocal frequency shift was measured from the reflection of the forward- and backward propagating probe [Fig. 15(d)].

Due to their strong, tunable resonances, high-index dielectric metasurfaces have proven to be a reliable platform for time-varying experiments. Although third-order nonlinearities in these materials are weaker than in ITO or AZO, and nanostructuring puts a lower cap on damage threshold and interaction volume, these metasurfaces can rival ENZ media due to the maturity of nanoantenna fabrication technology and the control of the scattering phase enabled by such systems.

5.2 New Leads for Time-Varying Metasurfaces

It is clear that better and more efficient material platforms for time-varying media are sought after and will likely appear in the near future, to allow for more efficient modulations, larger bandwidths, and higher damage thresholds. In this final section,

we identify a few promising candidates, namely quantum well polaritons, magneto-optical modulation, multilayered ENZ metamaterials, and 2D materials, exhibiting the potential to enhance time-modulation effects, and we discuss their respective strengths and weaknesses.

5.2.1 Quantum well polaritons

Mann et al.[238] showed in 2021 the pulse-limited modulation of intersubband polaritonic metasurfaces using the coupling between patch antennas and intersubband transitions in multiquantum wells (MQWs). The antenna resonance matches the transition dipole moment of the MQWs, which leads to Rabi splitting at low intensities. As the intensity increases, the ground state is depleted, which induces a change in coupling and absorption properties. The system operates at intensities between 70 and 700 kW/cm^2, with a change in absorption on the order of unity at the resonant frequency of the antenna. Although the change in reflection is quite weak at such powers (at best 8% here), it is worth noting that the intensities here are much lower than those used in other nonlinear optical experiments for time-modulation. On the other hand, the recovery time is dictated by the relaxation time of the excited state of the MQWs, here of 1.7 ps. In comparison, the modulation recovery time in unsaturated ITO is 360 fs.[211]

5.2.2 Magneto-optical modulation

Although the mutual effects of electric and magnetic fields are quite weak, one can consider using the magneto-optical Kerr effect (MOKE) or Faraday effect (MOFE) to achieve ultrafast time-dynamics and thus time-varying physics in a magnetic medium. MOKE (MOFE) consists in the rotation of reflected (transmitted) light by a magnetic field.[239,240] A first stone was laid when Beaurepaire et al.[241] showed in 1996 sub-ps switching of spin in ferromagnets using a MOKE configuration. Ultrafast spin switching was demonstrated without magnetic fields using a circularly polarized optical pulse,[242] exploiting the dynamics of the inverse Faraday effect. Particularly, Stanciu et al.[243] demonstrated a 40-fs all-optical switching of magnetization. Though in this experiment the origin of the switching was finally found out to be originating from the heating of the medium by the laser pulses, Mangin et al.[244] later showed helicity-dependent switching in various magnetic media, independently of the threshold switching temperature of the medium. This opened a new path toward ultrafast magnetic memory writing and other applications of optical switching of magnets.

Experiments involving the use of a magnetic field use a common figure of merit, the δ parameter, defined as the percentage change of reflection when the magnetization is reversed. That is for a magnetic field **M** and a reflection R, $\delta = [R(\mathbf{M}) - R(-\mathbf{M})]/R(\mathbf{0})$. This value is usually quite low in bulk ferromagnetic thin films, ranging from 10^{-5} to 10^{-3}. Nanostructuring can help increase this figure of merit: the coupling of surface plasmon polaritons from an Au grating to a ferromagnetic substrate allows for a stronger MOKE effect,[245] leading to a δ parameter of up to 24%.[246] In other works, plasmonic antennas in a magnetic field were used to control the transmission of chiral light,[247] and dielectric nanoantennas were engineered via their electric and magnetic Mie resonances to achieve a large Faraday rotation.[248] Yet, these time-modulations of the medium linked to the value of δ do require a switching of the magnetization, which happens on a much slower scale (100 ps to ns)[247,249] than the optical modulation from the MOKE itself. Hence, the ultrafast aspect of the modulation may only come from the rotation of the polarization of light at a given, fixed magnetization.

In a parallel stream of research, ultrafast spin currents have been excited in magnetized thin films and heterostructures using optical pulses, paving the way for THz emitter technologies.[250,251] Photocurrents were generated on a timescale of 330 fs in Huisman et al.'s work.[252] As the magnetic field does not require switching and can be maintained constant, the modulation can be considered as entirely optical and ultrafast. Qiu et al. demonstrated similar spin current generation in an antiferromagnetic slab in the absence of a magnetic field,[253] due to second-order optical nonlinearities. For a more detailed review of THz emitters and wave generation, the authors recommend the review by Feng et al.[254] While the potential of magneto-optical effects for ultrafast phenomena has been demonstrated, their translation into the framework of time-varying media remains unexplored, which calls for a new push in investigations and experiments in this direction.

5.2.3 Multilayered metamaterials

Multilayered metal–dielectric structures are of great interest due to their tunability to different regimes via fabrication, such as ENZ or hyperbolic. In addition, their simple architecture for fabrication is well-understood from effective-medium theory.[255]

Artificial ENZ metamaterials exhibiting Dirac cone-like dispersion[256] or multilayered thin films make valuable candidates for time-varying experiments, as they exhibit the favorable ENZ physics, are tunable, and have the potential to exploit other meta-properties, e.g., good coupling to far-field radiation. Sub-ps modulation of the effective permittivity of a multilayered Au/TiO$_2$ metamaterial was demonstrated by Rashed et al.[257] In parallel, enhancement of nonlinear properties around the ENZ frequency of a multilayered Ag/SiO$_2$[258] as well as ultrafast modulation of absorption[259] were reported. This enhancement is explained by the dependence of the effective third-order nonlinear susceptibility on the inverse of the medium's effective index, which reaches a minimum in the vicinity of the multilayered structure's ENZ frequency. In a similar spirit, ultrafast modulation of a metal–insulator–metal nanocavity was observed around the low-energy ENZ point,[260] but it was found that the switching speed was limited by the carrier density and heat capacity of the metal. The authors suggested the use of TCO-dielectric structures to accelerate the electron dynamics of the process and achieve faster modulation. Alternatively, multilayered ENZ metamaterials can be used to pin down and control the plasmonic resonance of coupled antennas depending on the ENZ frequency,[261] with optical modulation allowing for control of the antenna resonance via the multilayered substrate.

In a different paradigm, multilayered metal–dielectric antennas have been engineered to support ultrasmall mode volumes,[262] and in this way couple light efficiently to a WS$_2$ monolayer.[263] WS$_2$ and 2D materials are a promising class of media for time-varying experiments, as we discuss in the following section. Although monolayers feature properties favorable to modulation, their intrinsic atomic-scale thickness limits their coupling to light: hyperbolic metamaterials, such as a multilayered metal–dielectric antenna can overcome this barrier and boost optical modulation. Furthermore, efficient second and third harmonic generation was measured from multilayered Au/SiO$_2$ nanoantennas.[264] The efficiency of the second harmonic was proved to originate from the multiple metal–dielectric interfaces rather than symmetry-breaking, allowing for a polarization-independent implementation of multilayered antennas. Finally, magneto-optical effects have also been observed in similar hyperbolic nanoparticles,[265] opening a path toward magneto-optical modulation of multilayered antennas.

To sum up, multilayered ENZ metamaterials constitute promising candidates for time-varying experiments as they exhibit ultrafast modulation and strong nonlinear properties, while offering options for nanostructuring and resonance engineering.

5.2.4 2D materials

A modern topic in nanophotonics, 2D materials exhibit many interesting properties including high refractive index and ease of nanostructuring,[266] unconventional band structure and carrier dynamics such as Dirac cones,[267] and excitonic physics as well as ultrahigh carrier mobility,[268] resulting in strong optical nonlinearities useful for material modulation.[269,270] Transition metal dichalcogenides (TMDs), black phosphorus (BP), and graphene feature sub-ps carrier excitation times[271–273] in single layer structures. In particular, TMDs offer excitonic resonances with short recombination times, while monolayer BP exhibits a tunable direct bandgap from the visible to the mid-IR. In addition, BP's anisotropic response has also been shown to undergo modulation under laser excitation.[274] TMDs exhibit a variety

of useful properties for optical modulation,[275] with monolayer and low-dimensional TMDs exhibiting stronger nonlinear properties than their bulk counterparts. In Nie et al.'s work,[276] a 10-fs pulse of about 1 GW/cm^2 was shown to excite photocarriers in 20 fs in low-dimensional MoS$_2$, though the change in transmission was only of 0.8%. Large second- and third-order nonlinearities have also been measured in low dimensional MoS$_2$,[277,278] MoSe$_2$,[279] WS$_2$,[280,281] and WSe$_2$,[282] as well as a strong tunability of the refractive index in WSe$_2$, MoSe$_2$, and MoS$_2$.[283] In addition, the strong nonlinear properties in MoSe$_2$ can be exploited due to the comparatively high damage threshold of the monolayer as demonstrated by Tam et al.[279] Ultimately, applications are limited by the low-dimensionality of these materials, which leads to a small interaction volume and short interaction time. On the other hand, nanostructuring can again be used to enhance the response from these systems: enhanced light–matter interaction has been shown in monolayers coupled with plasmonic nanoantennas[284–286] as well as with a Si waveguide.[287] Nonlinear antennas built from bulk TMDs could also provide a platform for time-varying experiments in the same fashion as GaAs or Si.[288] Another alternative would be van der Waals heterostructures, stacked layers of TMDs that have also exhibited short rise times of about 50 fs,[289,290] with no dependence of the response time on the twisting angle between layers.[291,292] More information on the specific spin and valley dynamics at the origin of the ultrafast dynamics in van der Vaals heterostructures can be found in Jin et al.'s review.[293]

5.3 Outlook

All-optical implementations of time-varying metasurfaces are of great interest for the creation of new miniaturized technologies for the control of light both in space and time. ENZ materials such as ITO and AZO, along with high-index dielectrics, have proven to be solid platforms for time-varying experiments and will surely lay the ground for more complex investigations. These nanophotonic architectures can boost both light coupling to the nonlinear medium and field enhancement. Multilayered ENZ metamaterials could provide new solutions to the practical problems posed by the nature of more classical time-varying systems, such as resonance-engineering or high permittivity contrast. New materials and systems could pave the way for further development of time-varying experiments, expanding the spectral range of operation, increasing the efficiency and the damage threshold. Quantum well polaritons and monolayer 2D materials could exhibit time-varying effects at lower energies, while magneto-optical effects would open a new framework including time-varying magnetic effects, which are ignored in current nonlinear optical experiments.

6 Conclusions

In this review article, we have presented a comprehensive overview of photonic time-varying media. We started by reviewing the basic phenomenological and mathematical considerations rooted in the behavior of Maxwell's equations in the presence of temporal material discontinuities, discussing the main directions of ongoing research on electromagnetic time-switching for several applications, such as time-reversal, energy manipulation, frequency conversion, bandwidth enhancement, and wave routing, among many others. We then continued our discussion to consider PTCs, discussing the basic phenomenology underlying periodic time-scattering and parametric amplification to develop

an insight that we deployed in addressing more advanced instances of time-modulation, in particular for topological physics, non-Hermitian systems, and temporal disorder, concluding with some brief remarks on time-modulated surfaces. We then extended our discussion to combinations of spatial and temporal degrees of freedom, providing an overview of the basic properties of space–time crystals, and their application to nonreciprocity, as well as the engineering of synthetic motion and its applications to optical drag and giant bianisotropic responses, highlighting the concept of luminal amplification and spatiotemporal localization as a new form of wave amplification physically distinct from the conventional parametric gain, and concluding with an overview of the wealth of opportunities and applications for space–time metasurfaces. Finally, we reviewed some of the most successful materials and paradigms for experimental realizations of time-varying effects in the visible and IR, indicating some of the most promising avenues recently unveiled for future optical experiments with time-varying media. While the latter undoubtedly constitute the greatest long-term challenge for this rising field of research, we believe that, as in many other instances of scientific enquiry, the quest for time-varying photonic systems will prove a prolific one from both the point of view of unveiling and demonstrating fundamentally novel wave phenomena and for revealing new and unexpected windows of opportunity for technological advancement.

References

1. E. Knox and A. Wilson, Eds., *The Routledge Companion to Philosophy of Physics*, 1st ed., Taylor and Francis Group, p. 786, New York (2021).
2. R. Schützhold and W. G. Unruh, "Hawking radiation in an electromagnetic waveguide?" *Phys. Rev. Lett.* **95**(3), 031301 (2005).
3. T. G. Philbin et al., "Fiber-optical analog of the event horizon," *Science* **319**(5868), 1367–1370 (2008).
4. A. Shapere and F. Wilczek, "Classical time crystals," *Phys. Rev. Lett.* **109**(16), 160402 (2012).
5. K. Sacha and J. Zakrzewski, "Time crystals: a review," *Rep. Prog. Phys.* **81**(1), 016401 (2018).
6. N. Y. Yao et al., "Classical discrete time crystals," *Nat. Phys.* **16**(4), 438–447 (2020).
7. H. Keßler et al., "Observation of a dissipative time crystal," *Phys. Rev. Lett.* **127**(4), 043602 (2021).
8. N. Engheta, "Metamaterials with high degrees of freedom: space, time, and more," *Nanophotonics* **10**(1), 639–642 (2020).

9. L. Novotny and B. Hecht, *Principles of Nano-Optics*, Cambridge University Press (2012).

10. B. E. Saleh and M. C. Teich, *Fundamentals of Photonics*, John Wiley and Sons, Hoboken, New Jersey (2019).

11. R. W. Boyd, *Nonlinear Optics*, Academic Press, Cambridge, Massachusetts (2020).

12. V. G. Veselago, "Electrodynamics of substances with simultaneously negative electrical and magnetic permeabilities," *Sov. Phys. Usp.* **10**(4), 504–509 (1968).

13. J. B. Pendry, "Negative refraction makes a perfect lens," *Phys. Rev. Lett.* **85**(18), 3966–3969 (2000).

14. A. Alù et al., "Epsilon-near-zero metamaterials and electromagnetic sources: tailoring the radiation phase pattern," *Phys. Rev. B* **75**(15), 155410 (2007).

15. A. K. Iyer, A. Alù, and A. Epstein, "Metamaterials and metasurfaces—historical context, recent advances, and future directions," *IEEE Trans. Antennas Propag.* **68**(3), 1223–1231 (2020).

16. F. R. Morgenthaler, "Velocity modulation of electromagnetic waves," *IRE Trans. Microwave Theory Tech.* **6**(2), 167–172 (1958).

17. J. T. Mendonça, *Theory of Photon Acceleration*, CRC Press, Boca Raton, Florida (2000).

18. J. D. Jackson, *Classical Electrodynamics*, John Wiley and Sons, Hoboken, New Jersey (2012).

19. B. Auld, J. H. Collins, and H. Zapp, "Signal processing in a non-periodically time-varying magnetoelastic medium," *Proc. IEEE* **56**(3), 258–272 (1968).

20. R. Fante, "Transmission of electromagnetic waves into time-varying media," *IEEE Trans. Antennas Propag.* **19**(3), 417–424 (1971).

21. R. Fante, "On the propagation of electromagnetic waves through a time-varying dielectric layer," *Appl. Sci. Res.* **27**(1), 341–354 (1973).

22. P. Mukherjee and S. Talwar, "Reflection and transmission of electromagnetic waves at a moving magnetoplasma half-space," *Radio Sci.* **8**(7), 653–665 (1973).

23. Y. Xiao, D. N. Maywar, and G. P. Agrawal, "Reflection and transmission of electromagnetic waves at a temporal boundary," *Opt. Lett.* **39**(3), 574–577 (2014).

24. M. A. Salem and C. Caloz, "Space-time cross-mapping and application to wave scattering," arXiv 1504.02012 (2015).

25. C. Caloz and Z.-L. Deck-Léger, "Spacetime metamaterials—part II: theory and applications," *IEEE Trans. Antennas Propag.* **68**(3), 1583–1598 (2020).

26. M. Bakunov and A. Maslov, "Reflection and transmission of electromagnetic waves at a temporal boundary: comment," *Opt. Lett.* **39**(20), 6029 (2014).

27. D. K. Kalluri, *Electromagnetics of Time Varying Complex Media: Frequency and Polarization Transformer*, CRC Press, Boca Raton, Florida (2018).

28. A. Akbarzadeh, N. Chamanara, and C. Caloz, "Inverse prism based on temporal discontinuity and spatial dispersion," *Opt. Lett.* **43**(14), 3297–3300 (2018).

29. M. Bakunov et al., "Light scattering at a temporal boundary in a Lorentz medium," *Opt. Lett.* **46**(19), 4988–4991 (2021).

30. D. M. Solís, R. Kastner, and N. Engheta, "Time-varying materials in the presence of dispersion: plane-wave propagation in a Lorentzian medium with temporal discontinuity," *Photon. Res.* **9**(9), 1842–1853 (2021).

31. J. Gratus et al., "Temporal boundaries in electromagnetic materials," *New J. Phys.* **23**(8), 083032 (2021).

32. J. Zhang, W. Donaldson, and G. Agrawal, "Temporal reflection and refraction of optical pulses inside a dispersive medium: an analytic approach," *J. Opt. Soc. Am. B* **38**(3), 997–1003 (2021).

33. J. Zhang, W. Donaldson, and G. P. Agrawal, "Time-domain Fabry–Perot resonators formed inside a dispersive medium," *J. Opt. Soc. Am. B* **38**(8), 2376–2382 (2021).

34. K. Sacha, "Modeling spontaneous breaking of time-translation symmetry," *Phys. Rev. A* **91**(3), 033617 (2015).

35. D. V. Else, B. Bauer, and C. Nayak, "Floquet time crystals," *Phys. Rev. Lett.* **117**(9), 090402 (2016).

36. N. Y. Yao et al., "Discrete time crystals: rigidity, criticality, and realizations," *Phys. Rev. Lett.* **118**(3), 030401 (2017).

37. V. Pacheco-Peña and N. Engheta, "Temporal metamaterials with gain and loss," arXiv 2108.01007 (2021).

38. J. Mendonça, A. Martins, and A. Guerreiro, "Temporal beam splitter and temporal interference," *Phys. Rev. A* **68**(4), 043801 (2003).

39. V. Pacheco-Peña and N. Engheta, "Antireflection temporal coatings," *Optica* **7**(4), 323–331 (2020).

40. H. Li et al., "Temporal parity-time symmetry for extreme energy transformations," *Phys. Rev. Lett.* **127**(15), 153903 (2021).

41. D. M. Pozar, *Microwave Engineering*, John Wiley and Sons, Hoboken, New Jersey (2011).

42. D. Christodoulides et al., *Parity-Time Symmetry and Its Applications*, Vol. **280**, Springer, Singapore (2018).

43. V. Pacheco-Peña and N. Engheta, "Temporal aiming," *Light Sci. Appl.* **9**(1), 129 (2020).

44. V. Pacheco-Peña and N. Engheta, "Temporal Brewster angle," *Phys. Rev. B* **104**(21), 214308 (2021).

45. J. Xu, W. Mai, and D. H. Werner, "Complete polarization conversion using anisotropic temporal slabs," *Opt. Lett.* **46**(6), 1373–1376 (2021).

46. Z. Hayran, A. Chen, and F. Monticone, "Spectral causality and the scattering of waves," *Optica* **8**(8), 1040–1049 (2021).

47. D. M. Sols and N. Engheta, "Functional analysis of the polarization response in linear time-varying media: a generalization of the Kramers–Kronig relations," *Phys. Rev. B* **103**(14), 144303 (2021).

48. E. Yablonovitch, "Spectral broadening in the light transmitted through a rapidly growing plasma," *Phys. Rev. Lett.* **31**(14), 877–879 (1973).

49. E. Yablonovitch, "Self-phase modulation of light in a laser-breakdown plasma," *Phys. Rev. Lett.* **32**(20), 1101–1104 (1974).

50. C.-L. Jiang, "Wave propagation and dipole radiation in a suddenly created plasma," *IEEE Trans. Antennas Propag.* **23**(1), 83–90 (1975).

51. S. Wilks, J. Dawson, and W. Mori, "Frequency up-conversion of electromagnetic radiation with use of an overdense plasma," *Phys. Rev. Lett.* **61**(3), 337–340 (1988).

52. V. Bacot et al., "Time reversal and holography with spacetime transformations," *Nat. Phys.* **12**(10), 972–977 (2016).

53. G. A. Menendez and B. Maes, "Time reflection and refraction of graphene plasmons at a temporal discontinuity," *Opt. Lett.* **42**(23), 5006–5009 (2017).

54. J. Wilson et al., "Temporal control of graphene plasmons," *Phys. Rev. B* **98**(8), 081411 (2018).

55. A. Maslov and M. Bakunov, "Temporal scattering of a graphene plasmon by a rapid carrier density decrease," *Optica* **5**(12), 1508–1515 (2018).

56. A. Shlivinski and Y. Hadad, "Beyond the Bode-Fano bound: wideband impedance matching for short pulses using temporal switching of transmission-line parameters," *Phys. Rev. Lett.* **121**(20), 204301 (2018).

57. H. Li and A. Alù, "Temporal switching to extend the bandwidth of thin absorbers," *Optica* **8**(1), 24–29 (2021).

58. Y. Mazor, M. Cotrufo, and A. Alù, "Unitary excitation transfer between coupled cavities using temporal switching," *Phys. Rev. Lett.* **127**(1), 013902 (2021).

59. V. Pacheco-Peña and N. Engheta, "Spatiotemporal isotropic-to-anisotropic meta-atoms," *New J. Phys.* **23**(9), 095006 (2021).

60. F. Miyamaru et al., "Ultrafast frequency-shift dynamics at temporal boundary induced by structural-dispersion switching of waveguides," *Phys. Rev. Lett.* **127**(5), 053902 (2021).

61. W. Mori et al., "Conversion of DC fields in a capacitor array to radiation by a relativistic ionization front," *Phys. Rev. Lett.* **74**(4), 542–545 (1995).

62. M. Cirone, K. Rzaz-Dotewski, and J. Mostowski, "Photon generation by time-dependent dielectric: a soluble model," *Phys. Rev. A* **55**(1), 62–66 (1997).

63. M. J. Mencagli et al., "Static-to-dynamic field conversion with time-varying media," arXiv:2107.11420 (2021).

64. G. Ptitcyn, M. S. Mirmoosa, and S. A. Tretyakov, "Time-modulated meta-atoms," *Phys. Rev. Res.* **1**(2), 023014 (2019).

65. M. S. Mirmoosa et al., "Dipole polarizability of time-varying particles," arXiv:2002.12297 (2020).

66. G. Ptitcyn et al., "Scattering from spheres made of time-varying and dispersive materials," arXiv:2110.07195 (2021).

67. J. Tunesi et al., "Terahertz emission mediated by ultrafast time-varying metasurfaces," *Phys. Rev. Res.* **3**(4), L042006 (2021).

68. L. Stefanini et al., "Temporal interfaces and metamaterial response enabled by boundaries," arXiv:2105.14350 (2021).

69. J. R. Sanmartn, "O botafumeiro: parametric pumping in the middle ages," *Am. J. Phys.* **52**(10), 937–945 (1984).

70. F. Wilczek, "Quantum time crystals," *Phys. Rev. Lett.* **109**(16), 160401 (2012).

71. K. Sacha, *Time Crystals*, Springer, Cham, Switzerland (2020).

72. E. Lustig, Y. Sharabi, and M. Segev, "Topological aspects of photonic time crystals," *Optica* **5**(11), 1390–1395 (2018).

73. D. Torrent, W. J. Parnell, and A. N. Norris, "Loss compensation in time-dependent elastic metamaterials," *Phys. Rev. B* **97**(1), 014105 (2018).

74. D. Ramaccia et al., "Temporal multilayer structures for designing higher-order transfer functions using time-varying metamaterials," *Appl. Phys. Lett.* **118**(10), 101901 (2021).

75. G. Castaldi et al., "Exploiting space-time duality in the synthesis of impedance transformers via temporal metamaterials," *Nanophotonics* **10**(14), 3687–3699 (2021).

76. J. G. Gaxiola-Luna and P. Halevi, "Temporal photonic (time) crystal with a square profile of both permittivity ε(t) and permeability μ (t)," *Phys. Rev. B* **103**(14), 144306 (2021).

77. L. Yuan, A. Dutt, and S. Fan, "Synthetic frequency dimensions in dynamically modulated ring resonators," *APL Photonics* **6**(7), 071102 (2021).

78. L. Yuan et al., "Synthetic dimension in photonics," *Optica* **5**(11), 1396–1405 (2018).

79. L. Yuan, Y. Shi, and S. Fan, "Photonic gauge potential in a system with a synthetic frequency dimension," *Opt. Lett.* **41**(4), 741–744 (2016).

80. A. Dutt et al., "A single photonic cavity with two independent physical synthetic dimensions," *Science* **367**(6473), 59–64 (2020).

81. C. W. Peterson et al., "Strong nonreciprocity in modulated resonator chains through synthetic electric and magnetic fields," *Phys. Rev. Lett.* **123**(6), 063901 (2019).

82. J. S. Hung et al., "Quantum simulation of the bosonic Creutz ladder with a parametric cavity," *Phys. Rev. Lett.* **127**(10), 100503 (2021).

83. A. Dutt et al., "Experimental demonstration of dynamical input isolation in nonadiabatically modulated photonic cavities," *ACS Photonics* **6**(1), 162–169 (2019).

84. M. Zhang et al., "Electronically programmable photonic molecule," *Nat. Photonics* **13**(1), 36–40 (2019).

85. X. Ni, S. Kim, and A. Alù, "Topological insulator in two synthetic dimensions based on an optomechanical resonator," *Optica* **8**(8), 1024–1032 (2021).

86. T. T. Koutserimpas and R. Fleury, "Nonreciprocal gain in non-Hermitian time-Floquet systems," *Phys. Rev. Lett.* **120**(8), 087401 (2018).

87. R. Carminati et al., "Universal statistics of waves in a random time-varying medium," *Phys. Rev. Lett.* **127**(9), 4101 (2021).

88. T. T. Koutserimpas, A. Alù, and R. Fleury, "Parametric amplification and bidirectional invisibility in PT-symmetric time-Floquet systems," *Phys. Rev. A* **97**(1), 013839 (2018).

89. F. M. Arscott, "*Theory and Application of Mathieu Functions*. By N. W. Mclachlan. pp. xii, 401. (Dover, New York.)," *Math. Gaz.* **52**(379), 94–95 (1968).

90. N. Wang, Z.-Q. Zhang, and C. T. Chan, "Photonic Floquet media with a complex time-periodic permittivity," *Phys. Rev. B* **98**(8), 085142 (2018).

91. A. Bossart and R. Fleury, "Non-Hermitian time evolution: from static to parametric instability," *Phys. Rev. A* **104**(4), 2225 (2021).

92. T. T. Koutserimpas and R. Fleury, "Electromagnetic fields in a time-varying medium: exceptional points and operator symmetries," *IEEE Trans. Antennas Propag.* **68**(9), 6717–6724 (2020).

93. M. Li et al., "Topological phases and nonreciprocal edge states in non-Hermitian Floquet insulators," *Phys. Rev. B* **100**(4), 045423 (2019).

94. K. Wang et al., "Topological complex-energy braiding of non-Hermitian bands," *Nature* **598**(7879), 59–64 (2021).

95. S. Horsley, M. Artoni, and G. La Rocca, "Spatial Kramers–Kronig relations and the reflection of waves," *Nat. Photonics* **9**(7), 436–439 (2015).

96. B. Apffel et al., "Time localization of energy in disordered time-modulated systems," arXiv:2102.07583 (2021).

97. Y. Sharabi, E. Lustig, and M. Segev, "Disordered photonic time crystals," *Phys. Rev. Lett.* **126**(16), 163902 (2021).

98. J. Pendry, "The evolution of waves in disordered media," *J. Phys. C Solid State Phys.* **15**(16), 3493–3511 (1982).

99. U. C. Fischer and D. Pohl, "Observation of single-particle plasmons by near-field optical microscopy," *Phys. Rev. Lett.* **62**(4), 458–461 (1989).

100. R. W. Wood, "XLII. On a remarkable case of uneven distribution of light in a diffraction grating spectrum," *London Edinburgh Dublin Philos. Mag. J. Sci.* **4**(21), 396–402 (1902).

101. E. Galiffi et al., "Wood anomalies and surface-wave excitation with a time grating," *Phys. Rev. Lett.* **125**(12), 127403 (2020).

102. Z. Wu and A. Grbic, "Serrodyne frequency translation using time-modulated metasurfaces," *IEEE Trans. Antennas Propag.* **68**(3), 1599–1606 (2020).

103. R. C. Cumming, "The serrodyne frequency translator," *Proc. IRE* **45**(2), 175–186 (1957).

104. X. Wang et al., "Theory and design of multifunctional space-time metasurfaces," *Phys. Rev. Appl.* **13**(4), 044040 (2020).

105. D. Ramaccia et al., "Phase-induced frequency conversion and Doppler effect with time-modulated metasurfaces," *IEEE Trans. Antennas Propag.* **68**(3), 1607–1617 (2020).

106. C. Scarborough, Z. Wu, and A. Grbic, "Efficient computation of spatially discrete traveling-wave modulated structures," *IEEE Trans. Antennas Propag.* **69**(12), 8512–8525 (2021).

107. Z. Wu, C. Scarborough, and A. Grbic, "Space-time-modulated metasurfaces with spatial discretization: free-space *n*-path systems," *Phys. Rev. Appl.* **14**(6), 064060 (2020).

108. X. Wang et al., "Space–time metasurfaces for power combining of waves," *ACS Photonics* **8**(10), 3034–3041 (2021).

109. D. Ramaccia et al., "Electromagnetic isolation induced by time-varying metasurfaces: nonreciprocal Bragg grating," *IEEE Antennas Wirel. Propag. Lett.* **19**(11), 1886–1890 (2020).

110. H. B. Sedeh, M. M. Salary, and H. Mosallaei, "Time-varying optical vortices enabled by time-modulated metasurfaces," *Nanophotonics* **9**(9), 2957–2976 (2020).

111. Y. Hadad, D. L. Sounas, and A. Alù, "Space-time gradient metasurfaces," *Phys. Rev. B* **92**(10), 100304 (2015).

112. J. S. Martínez-Romero and P. Halevi, "Parametric resonances in a temporal photonic crystal slab," *Phys. Rev. A* **98**(5), 053852 (2018).

113. L. Zhang et al., "A wireless communication scheme based on space- and frequency-division multiplexing using digital metasurfaces," *Nat. Electron.* **4**(3), 218–227 (2021).

114. L. Zhang et al., "Space-time-coding digital metasurfaces," *Nat. Commun.* **9**, 4334 (2018).

115. A. M. Shaltout et al., "Spatiotemporal light control with frequency-gradient metasurfaces," *Science* **365**(6451), 374–377 (2019).

116. A. M. Shaltout, V. M. Shalaev, and M. L. Brongersma, "Spatiotemporal light control with active metasurfaces," *Science* **364**(6441), eaat3100 (2019).

117. X. Wang et al., "Nonreciprocity in bianisotropic systems with uniform time modulation," *Phys. Rev. Lett.* **125**(26), 266102 (2020).

118. J. S. Martínez-Romero, O. Becerra-Fuentes, and P. Halevi, "Temporal photonic crystals with modulations of both permittivity and permeability," *Phys. Rev. A* **93**(6), 063813 (2016).

119. Z.-L. Deck-Léger et al., "Uniform-velocity spacetime crystals," *Adv. Photonics* **1**(5), 056002 (2019).

120. E. Galiffi, P. A. Huidobro, and J. B. Pendry, "Broadband nonreciprocal amplification in luminal metamaterials," *Phys. Rev. Lett.* **123**(20), 206101 (2019).

121. D. L. Sounas and A. Alù, "Non-reciprocal photonics based on time modulation," *Nat. Photonics* **11**(12), 774–783 (2017).

122. J. Pierce, "Theory of the beam-type traveling-wave tube," *Proc. IRE* **35**(2), 111–123 (1947).

123. A. L. Cullen, "A travelling-wave parametric amplifier," *Nature* **181**(4605), 332 (1958).

124. A. Oliner and A. Hessel, "Wave propagation in a medium with a progressive sinusoidal disturbance," *IRE Trans. Microwave Theory Tech.* **9**(4), 337–343 (1961).

125. E. Cassedy and A. Oliner, "Dispersion relations in time-space periodic media—part I: stable interactions," *Proc. IEEE* **51**(10), 1342–1359 (1963).

126. E. Cassedy, "Dispersion relations in time-space periodic media—part II: unstable interactions," *Proc. IEEE* **55**(7), 1154–1168 (1967).

127. R. L. Fante, "Optical propagation in space–time-modulated media using many-space-scale perturbation theory," *J. Opt. Soc. Am.* **62**(9), 1052–1060 (1972).

128. J. N. Winn et al., "Interband transitions in photonic crystals," *Phys. Rev. B* **59**(3), 1551–1554 (1999).

129. F. Biancalana et al., "Dynamics of light propagation in spatiotemporal dielectric structures," *Phys. Rev. E* **75**(4), 046607 (2007).

130. S. Taravati, N. Chamanara, and C. Caloz, "Nonreciprocal electromagnetic scattering from a periodically space-time modulated slab and application to a quasisonic isolator," *Phys. Rev. B* **96**(16), 165144 (2017).

131. Y. Sivan, S. Rozenberg, and A. Halstuch, "Coupled-mode theory for electromagnetic pulse propagation in dispersive media undergoing a spatiotemporal perturbation: exact derivation, numerical validation, and peculiar wave mixing," *Phys. Rev. B* **93**(14), 144303 (2016).

132. Z. Yu and S. Fan, "Complete optical isolation created by indirect interband photonic transitions," *Nat. Photonics* **3**(2), 91–94 (2009).

133. H. Lira et al., "Electrically driven nonreciprocity induced by interband photonic transition on a silicon chip," *Phys. Rev. Lett.* **109**(3), 033901 (2012).

134. C. Caloz and Z.-L. Deck-Leger, "Spacetime metamaterials—part I: general concepts," *IEEE Trans. Antennas Propag.* **68**(3), 1569–1582 (2020).

135. E. Cassedy and A. Oliner, "Dispersion relations in time-space periodic media: part I–stable interactions," *Proc. IEEE* **51**(10), 1342 (1963).

136. D.-W. Wang et al., "Optical diode made from a moving photonic crystal," *Phys. Rev. Lett.* **110**(9), 093901 (2013).

137. N. Chamanara et al., "Optical isolation based on space-time engineered asymmetric photonic band gaps," *Phys. Rev. B* **96**(15), 155409 (2017).

138. D. L. Sounas, C. Caloz, and A. Alù, "Giant non-reciprocity at the subwavelength scale using angular momentum-biased metamaterials," *Nat. Commun.* **4**, 2407 (2013).

139. N. A. Estep et al., "Magnetic-free non-reciprocity and isolation based on parametrically modulated coupled-resonator loops," *Nat. Phys.* **10**(12), 923–927 (2014).

140. C. Caloz et al., "Electromagnetic nonreciprocity," *Phys. Rev. Appl.* **10**(4), 047001 (2018).

141. J. V. Bladel, *Relativity and Engineering*, Springer Verlag, Berlin (1984).

142. A. Fresnel, "Lettre d'augustin Fresnel à François Arago sur l'influence du mouvement terrestre dans quelques phénomènes d'optique," *Ann. Chim. Phys.* **9**, 57–66 (1818).

143. H. Fizeau, "Sur les hypotheses relatives à l'ether lumineux," *Comptes Rendus l'Acad. Sci.* **33**, 349 (1851).

144. J. A. Kong, *Electromagnetic Wave Theory*, EMW Publishing, Cambridge, Massachusetts (2008).

145. R. Fleury et al., "Sound isolation and giant linear nonreciprocity in a compact acoustic circulator," *Science* **343**(6170), 516–519 (2014).

146. S. Lannebère and M. G. Silveirinha, "Wave instabilities and unidirectional light flow in a cavity with rotating walls," *Phys. Rev. A* **94**(3), 033810 (2016).

147. J. B. Pendry, "Shearing the vacuum—quantum friction," *J. Phys. Condens. Matter.* **9**(47), 10301 (1997).

148. M. G. Silveirinha, "Theory of quantum friction," *New J. Phys.* **16**(6), 063011 (2014).

149. B. Shapiro, "Fluctuation-induced forces in the presence of mobile carrier drift," *Phys. Rev. B* **96**(7), 075407 (2017).

150. A. I. Volokitin and B. N. J. Persson, "Quantum friction," *Phys. Rev. Lett.* **106**(9), 094502 (2011).

151. Y. B. Zeldovich, "Generation of waves by a rotating body," *JETP Lett.* **14**(4), 180 (1971).

152. M. G. Silveirinha, "Optical instabilities and spontaneous light emission by polarizable moving matter," *Phys. Rev. X* **4**(3), 031013 (2014).

153. D. Faccio and E. M. Wright, "Nonlinear Zeldovich effect: parametric amplification from medium rotation," *Phys. Rev. Lett.* **118**(9), 093901 (2017).

154. V. K. O. Sydoruk, E. Shamonina, and L. Solymar, "Terahertz instability of surface optical-phonon polaritons that interact with surface plasmon polaritons in the presence of electron drift," *Phys Plasmas* **17**(10), 102103 (2010).

155. T. A. Morgado and M. G. Silveirinha, "Negative Landau damping in bilayer graphene," *Phys. Rev. Lett.* **119**(13), 133901 (2017).

156. B. V. Duppen et al., "Current-induced birefrigent absorption and non-reciprocal plasmons in graphene," *2D Mater.* **3**(1), 015011 (2016).

157. T. A. Morgado and M. G. Silveirinha, "Drift-induced unidirectional graphene plasmons," *ACS Photonics* **5**(11), 4253–4258 (2018).

158. B. Shapiro, "Thermal fluctuations of the electric field in the presence of carrier drift," *Phys. Rev. B* **82**(7), 075205 (2010).

159. Y. Dong et al., "Fizeau drag in graphene plasmonics," *Nature* **594**(7864), 513–516 (2021).

160. W. Zhao et al., "Efficient Fizeau drag from Dirac electrons in monolayer graphene," *Nature* **594**(7864), 517 (2021).

161. P. A. Huidobro et al., "Fresnel drag in space–time-modulated metamaterials," *Proc. Natl. Acad. Sci.* **116**(50), 24943–24948 (2019).

162. Y. Mazor and A. Alù, "One-way hyperbolic metasurfaces based on synthetic motion," *IEEE Trans. Antennas Propag.* **68**(3), 1739–1747 (2020).

163. P. A. Huidobro et al., "Homogenization theory of space-time metamaterials," *Phys. Rev. Appl.* **16**(1), 014044 (2021).

164. S. T. A. Serdyukov, I. Semchenko, and A. Sihvola, *Electromagnetics of Bianisotropic Materials Theory and Applications*, 1st ed., Gordon and Breach Science Publishers, Amsterdam (2001).

165. D. R. Smith and J. Pendry, "Homogenization of metamaterials by field averaging," *J. Opt. Soc. Am. B* **23**(3), 391–403 (2006).

166. M. G. Silveirinha, "Metamaterial homogenization approach with application to the characterization of microstructured composites with negative parameters," *Phys. Rev. B* **75**(11), 115104 (2007).

167. C. R. Simovski and S. A. Tretyakov, "Local constitutive parameters of metamaterials from an effective-medium perspective," *Phys. Rev. B* **75**(19), 195111 (2007).

168. A. Alù, "First-principles homogenization theory for periodic metamaterials," *Phys. Rev. B* **84**(7), 075153 (2011).

169. H. T. To, "Homogenization of dynamic laminates," *J. Math. Anal. Appl.* **354**(2), 518–538 (2009).

170. K. Lurie, *An Introduction to the Mathematical Theory of Waves*, Springer, New York (2007).

171. D. E. Aspnes, "Local-field effects and effective-medium theory: a microscopic perspective," *Am. J. Phys.* **50**(8), 704 (1982).

172. J. B. Pendry et al., "Magnetism from conductors and enhanced nonlinear phenomena," *IEEE Trans. Microwave Theory Technol.* **47**(11), 2075 (1999).

173. D. N. Astrov, "Magnetoelectric effect in chromium oxide," *Sov. Phys. JETP* **13**(4), 729 (1961).

174. S. Coh and D. Vanderbilt, "Canonical magnetic insulators with isotropic magnetoelectric coupling," *Phys. Rev. B* **88**(12), 121106 (2013).

175. S. Taravati, "Giant linear nonreciprocity, zero reflection, and zero band gap in equilibrated space-time-varying media," *Phys. Rev. Appl.* **9**(6), 064012 (2018).

176. E. Galiffi et al., "Photon localization and Bloch symmetry breaking in luminal gratings," *Phys. Rev. B* **104**(1), 014302 (2021).

177. E. Galiffi, "New degrees of freedom for metamaterials and metasurfaces: from hidden spatial dimensions to dynamical structures," PhD Thesis, Imperial College London (2020).

178. J. Pendry, E. Galiffi, and P. Huidobro, "Gain in time-dependent media—a new mechanism," *J. Opt. Soc. Am. B* **38**(11), 3360–3366 (2021).

179. J. Pendry, E. Galiffi, and P. Huidobro, "Gain mechanism in time-dependent media," *Optica* **8**(5), 636–637 (2021).

180. N. Chamanara, D. G. Cooke, and C. Caloz, "Linear pulse compansion based on space-time modulation," in *IEEE Int. Symp. Antennas and Propag. and USNC-URSI Radio Sci. Meeting*, IEEE, Atlanta, GA, pp. 239–240 (2019).

181. H. B. Sedeh, M. M. Salary, and H. Mosallaei, "Topological space-time photonic transitions in angular-momentum-biased metasurfaces," *Adv. Opt. Mater.* **8**(11), 2000075 (2020).

182. Y. Hadad, J. C. Soric, and A. Alù, "Breaking temporal symmetries for emission and absorption," *Proc. Natl. Acad. Sci.* **113**(13), 3471–3475 (2016).

183. A. Shaltout, A. Kildishev, and V. Shalaev, "Time-varying metasurfaces and Lorentz non-reciprocity," *Opt. Mater. Express* **5**(11), 2459–2467 (2015).

184. L. Zhang et al., "Breaking reciprocity with space-time-coding digital metasurfaces," *Adv. Mater.* **31**(41), 1904069 (2019).

185. H. Rajabalipanah et al., "Analog signal processing through space-time digital metasurfaces," *Nanophotonics* **10**(6), 1753–1764 (2021).

186. D. Oue, K. Ding, and J. Pendry, "Čerenkov radiation in vacuum from a superluminal grating," arXiv:2105.13681 (2021).

187. W. J. M. Kort-Kamp, A. K. Azad, and D. A. R. Dalvit, "Space-time quantum metasurfaces," *Phys. Rev. Lett.* **127**(4), 043603 (2021).

188. N. Chamanara et al., "Unusual electromagnetic modes in space-time-modulated dispersion-engineered media," *Phys. Rev. A* **97**(6), 063829 (2018).

189. D. Torrent, "Strong spatial dispersion in time-modulated dielectric media," *Phys. Rev. B* **102**(21), 214202 (2020).

190. E. Galiffi, P. A. Huidobro, and J. Pendry, "An Archimedes' screw for light," arXiv:2109.14460 (2021).

191. R. Fleury, A. B. Khanikaev, and A. Alù, "Floquet topological insulators for sound," *Nat. Commun.* **7**, 11744 (2016).

192. L. He et al., "Floquet Chern insulators of light," *Nat. Commun.* **10**, 4194 (2019).

193. K. Fang, Z. Yu, and S. Fan, "Photonic Aharonov–Bohm effect based on dynamic modulation," *Phys. Rev. Lett.* **108**(15), 153901 (2012).

194. Q. Lin et al., "Photonic Weyl point in a two-dimensional resonator lattice with a synthetic frequency dimension," *Nat. Commun.* **7**, 13731 (2016).

195. G. W. Milton and O. Mattei, "Field patterns: a new mathematical object," *Proc. R. Soc. A* **473**(2198), 20160819 (2017).

196. O. Mattei and G. W. Milton, "Field patterns without blow up," *New J. Phys.* **19**(9), 093022 (2017).

197. D. Torrent, O. Poncelet, and J.-C. Batsale, "Nonreciprocal thermal material by spatiotemporal modulation," *Phys. Rev. Lett.* **120**(12), 125501 (2018).

198. H. Nassar et al., "Quantization of band tilting in modulated phononic crystals," *Phys. Rev. B* **97**(1), 014305 (2018).

199. J. Li et al., "Transfer matrix method for the analysis of space-time-modulated media and systems," *Phys. Rev. B* **100**(14), 144311 (2019).

200. M. Camacho, B. Edwards, and N. Engheta, "Achieving asymmetry and trapping in diffusion with spatiotemporal metamaterials," *Nat. Commun.* **11**, 3733 (2020).

201. Y. Wang et al., "Observation of nonreciprocal wave propagation in a dynamic phononic lattice," *Phys. Rev. Lett.* **121**(19), 194301 (2018).

202. Z. Chen et al., "Efficient nonreciprocal mode transitions in spatiotemporally modulated acoustic metamaterials," *Sci. Adv.* **7**(45), eabj1198 (2021).

203. X. Xu et al., "Physical observation of a robust acoustic pumping in waveguides with dynamic boundary," *Phys. Rev. Lett.* **125**(25), 253901 (2020).

204. C. Cho et al., "Digitally virtualized atoms for acoustic metamaterials," *Nat. Commun.* **11**, 251 (2020).

205. X. Wen et al., "Unidirectional amplification with acoustic non-Hermitian space–time varying metamaterial," *Commun. Phys.* **5**, 18 (2022).

206. V. Bacot et al., "Phase-conjugate mirror for water waves driven by the Faraday instability," *Proc. Natl. Acad. Sci. U. S. A.* **116**(18), 8809–8814 (2019).

207. K. Schultheiss et al., "Time refraction of spin waves," *Phys. Rev. Lett.* **126**(13), 137201 (2021).

208. E. A. Kittlaus et al., "Non-reciprocal interband Brillouin modulation," *Nat. Photonics* **12**(10), 613–619 (2018).

209. Z. Shen et al., "Experimental realization of optomechanically induced non-reciprocity," *Nat. Photonics* **10**(10), 657–661 (2016).

210. N. Kinsey et al., "Near-zero-index materials for photonics," *Nat. Rev. Mater.* **4**(12), 742–760 (2019).

211. M. Z. Alam et al., "Large optical nonlinearity of indium tin oxide in its epsilon-near-zero region," *Science* **352**(6287), 795–797 (2016).

212. L. Caspani et al., "Enhanced nonlinear refractive index in ε-near-zero materials," *Phys. Rev. Lett.* **116**(23), 233901 (2016).

213. T. S. Luk et al., "Enhanced third harmonic generation from the epsilon-near-zero modes of ultrathin films," *Appl. Phys. Lett.* **106**(15), 151103 (2015).

214. E. G. Carnemolla et al., "Degenerate optical nonlinear enhancement in epsilon-near-zero transparent conducting oxides," *Opt. Mater. Express* **8**(11), 3392–3400 (2018).

215. Y. Zhou et al., "Broadband frequency translation through time refraction in an epsilon-near-zero material," *Nat. Commun.* **11**, 2180 (2020).

216. V. Bruno et al., "Broad frequency shift of parametric processes in epsilon-near-zero time-varying media," *Appl. Sci.* **10**(4), 1318 (2020).

217. V. Bruno et al., "Negative refraction in time-varying strongly coupled plasmonic-antenna–epsilon-near-zero systems," *Phys. Rev. Lett.* **124**(4), 043902 (2020).

218. K. Pang et al., "Adiabatic frequency conversion using a time-varying epsilon-near-zero metasurface," *Nano Lett.* **21**(14), 5907–5913 (2021).

219. M. Ferrera and E. G. Carnemolla, "Ultra-fast transient plasmonics using transparent conductive oxides," *J. Opt.* **20**(2), 024007 (2018).

220. S. Vezzoli et al., "Optical time reversal from time-dependent epsilon-near-zero media," *Phys. Rev. Lett.* **120**(4), 043902 (2018).

221. J. Bohn, T. S. Luk, and E. Hendry, "Spatiotemporal refraction of light in an epsilon-near-zero indium tin oxide layer: frequency shifting effects arising from interfaces," *Optica* **8**(12), 1532–1537 (2021).

222. C. Liu et al., "Photon acceleration using a time-varying epsilon-near-zero metasurface," *ACS Photonics* **8**(3), 716–720 (2021).

223. P. Guo et al., "Large optical nonlinearity of ITO nanorods for sub-picosecond all-optical modulation of the full-visible spectrum," *Nat. Commun.* **7**, 12892 (2016).

224. S. Vassant et al., "Berreman mode and epsilon near zero mode," *Opt. Express* **20**(21), 23971 (2012).

225. J. Bohn et al., "All-optical switching of an epsilon-near-zero plasmon resonance in indium tin oxide," *Nat. Commun.* **12**, 1017 (2021).

226. M. Z. Alam et al., "Large optical nonlinearity of nanoantennas coupled to an epsilon-near-zero material," *Nat. Photonics* **12**(2), 79–83 (2018).

227. Y. Yang et al., "High-harmonic generation from an epsilon-near-zero material," *Nat. Phys.* **15**(10), 1022–1026 (2019).

228. C. Husko et al., "Ultrafast all-optical modulation in GaAs photonic crystal cavities," *Appl. Phys. Lett.* **94**(2), 021111 (2009).

229. M. R. Shcherbakov et al., "Ultrafast all-optical switching with magnetic resonances in nonlinear dielectric nanostructures," *Nano Lett.* **15**(10), 6985–6990 (2015).

230. S. Makarov et al., "Tuning of magnetic optical response in a dielectric nanoparticle by ultrafast photoexcitation of dense electron–hole plasma," *Nano Lett.* **15**(9), 6187–6192 (2015).

231. G. Della Valle et al., "Nonlinear anisotropic dielectric metasurfaces for ultrafast nanophotonics," *ACS Photonics* **4**(9), 2129–2136 (2017).

232. M. R. Shcherbakov et al., "Ultrafast all-optical tuning of direct-gap semiconductor metasurfaces," *Nat. Commun.* **8**, 17 (2017).

233. G. Grinblat et al., "Efficient ultrafast all-optical modulation in a nonlinear crystalline gallium phosphide nanodisk at the anapole excitation," *Sci. Adv.* **6**(34), eabb3123 (2020).

234. R. Lemasters et al., "Deep optical switching on subpicosecond timescales in an amorphous Ge metamaterial," *Adv. Opt. Mater.* **9**(15), 2100240 (2021).

235. M. R. Shcherbakov et al., "Photon acceleration and tunable broadband harmonics generation in nonlinear time-dependent metasurfaces," *Nat. Commun.* **10**, 1345 (2019).

236. N. Karl et al., "Frequency conversion in a time-variant dielectric metasurface," *Nano Lett.* **20**(10), 7052–7058 (2020).

237. X. Guo et al., "Nonreciprocal metasurface with space–time phase modulation," *Light Sci. Appl.* **8**(1), 123 (2019).

238. S. A. Mann et al., "Ultrafast optical switching and power limiting in intersubband polaritonic metasurfaces," *Optica* **8**(5), 606–613 (2021).

239. N. Maccaferri et al., "Nanoscale magnetophotonics," *J. Appl. Phys.* **127**(8), 080903 (2020).

240. A. Kirilyuk, A. V. Kimel, and T. Rasing, "Ultrafast optical manipulation of magnetic order," *Rev. Mod. Phys.* **82**(3), 2731–2784 (2010).

241. E. Beaurepaire et al., "Ultrafast spin dynamics in ferromagnetic nickel," *Phys. Rev. Lett.* **76**(22), 4250–4253 (1996).

242. A. V. Kimel et al., "Ultrafast non-thermal control of magnetization by instantaneous photomagnetic pulses," *Nature* **435**(7042), 655–657 (2005).

243. C. D. Stanciu et al., "All-optical magnetic recording with circularly polarized light," *Phys. Rev. Lett.* **99**(4), 047601 (2007).

244. S. Mangin et al., "Engineered materials for all-optical helicity-dependent magnetic switching," *Nat. Mater.* **13**(3), 286–292 (2014).

245. V. I. Belotelov et al., "Enhanced magneto-optical effects in magnetoplasmonic crystals," *Nat. Nanotechnol.* **6**(6), 370–376 (2011).

246. V. I. Belotelov et al., "Plasmon-mediated magneto-optical transparency," *Nat. Commun.* **4**, 2128 (2013).

247. I. Zubritskaya et al., "Magnetic control of the chiroptical plasmonic surfaces," *Nano Lett.* **18**(1), 302–307 (2018).

248. A. Christofi et al., "Giant enhancement of faraday rotation due to electromagnetically induced transparency in all-dielectric magneto-optical metasurfaces," *Opt. Lett.* **43**(8), 1838–1841 (2018).

249. L. Landau and E. Lifshitz, "On the theory of the dispersion of magnetic permeability in ferromagnetic bodies," *Phys. Z. Sowjetunion* **8**, 153–164 (1935).

250. T. Kampfrath et al., "Coherent terahertz control of antiferromagnetic spin waves," *Nat. Photonics* **5**(1), 31–34 (2011).

251. T. Kampfrath et al., "Terahertz spin current pulses controlled by magnetic heterostructures," *Nat. Nanotechnol.* **8**(4), 256–260 (2013).

252. T. J. Huisman et al., "Femtosecond control of electric currents in metallic ferromagnetic heterostructures," *Nat. Nanotechnol.* **11**(5), 455–458 (2016).

253. H. Qiu et al., "Ultrafast spin current generated from an antiferromagnet," *Nat. Phys.* **17**(3), 388–394 (2021).

254. Z. Feng et al., "Spintronic terahertz emitter," *J. Appl. Phys.* **129**(1), 010901 (2021).

255. A. A. Orlov et al., "Controlling light with plasmonic multilayers," *Photonics Nanostruct. Fundam. Appl.* **12**(3), 213–230 (2014).

256. P. Moitra et al., "Realization of an all-dielectric zero-index optical metamaterial," *Nat. Photonics* **7**(10), 791–795 (2013).

257. A. R. Rashed et al., "Hot electron dynamics in ultrafast multilayer epsilon-near-zero metamaterials," *Phys. Rev. B* **101**(16), 165301 (2020).

258. S. Suresh et al., "Enhanced nonlinear optical responses of layered epsilon-near-zero metamaterials at visible frequencies," *ACS Photonics* **8**(1), 125–129 (2021).

259. J. N. Acharyya et al., "Ultrafast nonlinear pulse propagation dynamics in metal–dielectric periodic photonic architectures," *Adv. Mater. Interfaces* **8**(19), 2100757 (2021).

260. J. Kuttruff et al., "Ultrafast all-optical switching enabled by epsilon-near-zero-tailored absorption in metal-insulator nanocavities," *Commun. Phys.* **3**(1), 114 (2020).

261. M. Habib et al., "Controlling the plasmon resonance via epsilon-near-zero multilayer metamaterials," *Nanophotonics* **9**(11), 3637–3644 (2020).

262. S. R. K. C. Indukuri et al., "Ultrasmall mode volume hyperbolic nanocavities for enhanced light–matter interaction at the nanoscale," *ACS Nano* **13**(10), 11770–11780 (2019).

263. S. R. K. Indukuri et al., "WS_2 monolayers coupled to hyperbolic metamaterial nanoantennas: Broad implications for light–matter-interaction applications," *ACS Appl. Nano Mater.* **3**(10), 10226–10233 (2020).

264. N. Maccaferri et al., "Enhanced nonlinear emission from single multilayered metal–dielectric nanocavities resonating in the near-infrared," *ACS Photonics* **8**(2), 512–520 (2021).

265. J. Kuttruff et al., "Magneto-optical activity in nonmagnetic hyperbolic nanoparticles," *Phys. Rev. Lett.* **127**(21), 217402 (2021).

266. R. Verre et al., "Transition metal dichalcogenide nanodisks as high-index dielectric Mie nanoresonators," *Nat. Nanotechnol.* **14**(7), 679–683 (2019).

267. A. H. C. Neto et al., "The electronic properties of graphene," *Rev. Mod. Phys.* **81**(1), 109–162 (2009).

268. J. R. Schaibley et al., "Valleytronics in 2d materials," *Nat. Rev. Mater.* **1**(11), 16055 (2016).

269. J. You et al., "Nonlinear optical properties and applications of 2d materials: theoretical and experimental aspects," *Nanophotonics* **8**(1), 63–97 (2018).

270. S. Yu et al., "2D materials for optical modulation: challenges and opportunities," *Adv. Mater.* **29**(14), 1606128 (2017).

271. C. Poellmann et al., "Resonant internal quantum transitions and femtosecond radiative decay of excitons in monolayer WSe_2," *Nat. Mater.* **14**(9), 889–893 (2015).

272. E. A. A. Pogna et al., "Photo-induced bandgap renormalization governs the ultrafast response of single-layer MoS$_2$," *ACS Nano* **10**(1), 1182–1188 (2016).

273. K. Wang et al., "Ultrafast nonlinear excitation dynamics of black phosphorus nanosheets from visible to mid-infrared," *ACS Nano* **10**(7), 6923–6932 (2016).

274. S. Ge et al., "Dynamical evolution of anisotropic response in black phosphorus under ultrafast photoexcitation," *Nano Lett.* **15**(7), 4650–4656 (2015).

275. A. Autere et al., "Nonlinear optics with 2d layered materials," *Adv. Mater.* **30**(24), 1705963 (2018).

276. Z. Nie et al., "Ultrafast carrier thermalization and cooling dynamics in few-layer MoS$_2$," *ACS Nano* **8**(10), 10931–10940 (2014).

277. N. Kumar et al., "Second harmonic microscopy of monolayer MoS$_2$," *Phys. Rev. B* **87**(16), 161403 (2013).

278. A. Säynätjoki et al., "Ultra-strong nonlinear optical processes and trigonal warping in MoS$_2$ layers," *Nat. Commun.* **8**, 893 (2017).

279. C. T. Le et al., "Nonlinear optical characteristics of monolayer MoSe$_2$," *Ann. Phys., Lpz.* **528**(7-8), 551–559 (2016).

280. C. Janisch et al., "Extraordinary second harmonic generation in tungsten disulfide monolayers," *Sci. Rep.* **4**(1), 5530 (2014).

281. C. Torres-Torres et al., "Third order nonlinear optical response exhibited by mono- and few-layers of WS$_{2x}$," *2D Mater.* **3**(2), 021005 (2016).

282. J. Ribeiro-Soares et al., "Second harmonic generation in WSe$_2$," *2D Mater.* **2**(4), 045015 (2015).

283. G. Wang et al., "Tunable nonlinear refractive index of two-dimensional MoS$_2$, WS$_2$, and MoSe$_2$ nanosheet dispersions [invited]," *Photonics Res.* **3**(2), A51–A55 (2015).

284. J. Kern et al., "Nanoantenna-enhanced light–matter interaction in atomically thin WS$_{2x}$," *ACS Photonics* **2**(9), 1260–1265 (2015).

285. F. Spreyer et al., "Second harmonic imaging of plasmonic pancharatnam-berry phase metasurfaces coupled to monolayers of WS$_{2x}$," *Nanophotonics* **9**(2), 351–360 (2020).

286. X. Chen et al., "Resonance coupling in hybrid gold nanohole–monolayer WS$_{2x}$ nanostructures," *Appl. Mater. Today* **15**, 145–152 (2019).

287. H. Chen et al., "Enhanced second-harmonic generation from two-dimensional MoSe$_2$ on a silicon waveguide," *Light Sci. Appl.* **6**(10), e17060 (2017).

288. S. Busschaert et al., "Transition metal dichalcogenide resonators for second harmonic signal enhancement," *ACS Photonics* **7**(9), 2482–2488 (2020).

289. X. Hong et al., "Ultrafast charge transfer in atomically thin MoS$_2$/WS$_2$ heterostructures," *Nat. Nanotechnol.* **9**(9), 682–686 (2014).

290. F. Ceballos et al., "Ultrafast charge separation and indirect exciton formation in a MoS$_2$-MoSe$_2$ van der Waals heterostructure," *ACS Nano* **8**(12), 12717–12724 (2014).

291. K. Wang et al., "Interlayer coupling in twisted WSe$_2$/WS$_2$ bilayer heterostructures revealed by optical spectroscopy," *ACS Nano* **10**(7), 6612–6622 (2016).

292. H. Zhu et al., "Interfacial charge transfer circumventing momentum mismatch at two-dimensional van der Waals heterojunctions," *Nano Lett.* **17**(6), 3591–3598 (2017).

293. C. Jin et al., "Ultrafast dynamics in van der Waals heterostructures," *Nat. Nanotechnol.* **13**(11), 994–1003 (2018).

Emanuele Galiffi is a junior fellow of the Simons Society of Fellows, based at the Advanced Science Research Center of the City University of New York. After receiving his PhD in November 2020, he was an EPSRC Doctoral Prize Fellow at Imperial College London until August 2021. His research interests focus on exotic wave dynamics in time-varying materials and metamaterials, transformation optics, plasmonics, and polaritonics of low-symmetry materials.

Romain Tirole is a PhD candidate in Prof. Sapienza's Complex Nanophotonics Research Group at Imperial College London. His research interests cover waves in time-varying ENZ metasurfaces as well as dielectric nonlinear optical antennas. Before joining Imperial College, Romain worked on thermal lensing in gold nanoparticle suspensions for his master's thesis at the University of Cambridge's Nanophotonics Centre, and earned a BSc degree studying successively at the University of Toulouse and Imperial College London.

Shixiong Yin is a graduate assistant at the Advanced Science Research Center of the City University of New York. He has been pursuing his PhD in electrical engineering at City College of The City University of New York since 2019, after receiving a bachelor's degree in microwave engineering from Harbin Institute of Technology, China. He is now focusing on wave propagation in time-varying media, metamaterials, and plasmonics.

Huanan Li is a professor of physics at Nankai University. He received his BSc degree in physics from Sichuan University, China, in 2009 and his PhD in 2013 from National University of Singapore. Later, he studied as a postdoctoral researcher at Wesleyan University (2014–2018) and Photonics Initiative of CUNY Advanced Science Research Center (2018–2021) in USA. His research interests focus on wave physics and its methodology in non-Hermitian and time-varying systems.

Stefano Vezzoli is a research associate and a Strategic Teaching Fellow at Imperial College London since 2018. From 2020 he is working on an EPSRC New Horizon project grant titled 'Space-time metasurfaces for light waves. Before joining Imperial College, he worked as a Research Associate in Heriot-Watt University in Edinburgh, NTU in Singapore and Pierre and Marie University in Paris. His research interests include quantum optics, nonlinear optics, and metamaterials.

Paloma A. Huidobro received her PhD from Universidad Autónoma de Madrid (Spain) in 2013 and in 2014 joined Imperial College as a postdoctoral researcher, where she held a Marie Sklodowska-Curie Fellowship. In 2019 she took up an FCT Researcher Fellowship in Lisbon, where she is currently a researcher at Instituto de Telecomunicações, based in Instituto Superior Técnico–University of Lisbon. Her work is devoted to developing theory of nano-scale light-matter interactions, nanophotonics, and metamaterials.

Mário G. Silveirinha is a professor at the Instituto Superior Técnico–University of Lisbon, Portugal and a Senior Researcher at Instituto de Telecomunicações. He is an IEEE fellow, and OSA fellow, and an APS fellow. His research interests include electromagnetism, plasmonics and metamaterials, quantum optics, and topological effects.

Riccardo Sapienza works as professor of physics at Imperial College London, director of the Plasmonics and Metamaterials Centre. He received his PhD in physics joint from LENS, in the University of Florence and ENS, Paris XI. He conducted postdoctoral studies in Spain in ICMM-CSIC and in ICFO. His interests range from nanophotonics of complex media, single molecule spectroscopy, and metamaterials.

Andrea Alù is the Einstein Professor and founding director at the Photonics Initiative, Advanced Science Research Center, City University of New York. He received his MS and PhD degrees from the University of Roma Tre, Italy, and was the Temple Foundation Endowed Professor at the University of Texas at Austin until 2018. His research interests focus on metamaterials, electromagnetics, nanophotonics, and acoustics. He is a fellow of NAI, AAAS, IEEE, Optica, APS, MRS, and SPIE.

J. B. Pendry is a condensed matter theorist and has worked at Imperial College London since 1981. He has worked extensively on electronic and structural properties of surfaces developing the theory of low energy diffraction. He then turned his attention to photonic materials and designed a series of metamaterials, completely novel materials with properties not found in nature giving rise to the first material with a negative refractive index and a prototype cloaking device.